AFRL-RX-WP-TP-2012-0373

POROSITY EVOLUTION IN A CREEPING SINGLE CRYSTAL (PREPRINT)

A. **Srivastava and A. Needleman**
University of North Texas

August 2012
Interim

Approved for public release; distribution unlimited.

See additional restrictions described on inside pages

STINFO COPY

AIR FORCE RESEARCH LABORATORY
MATERIALS AND MANUFACTURING DIRECTORATE
WRIGHT-PATTERSON AIR FORCE BASE, OH 45433-7750
AIR FORCE MATERIEL COMMAND
UNITED STATES AIR FORCE

REPORT DOCUMENTATION PAGE

Form Approved
OMB No. 0704-0188

The public reporting burden for this collection of information is estimated to average 1 hour per response, including the time for reviewing instructions, searching existing data sources, searching existing data sources, gathering and maintaining the data needed, and completing and reviewing the collection of information. Send comments regarding this burden estimate or any other aspect of this collection of information, including suggestions for reducing this burden, to Department of Defense, Washington Headquarters Services, Directorate for Information Operations and Reports (0704-0188), 1215 Jefferson Davis Highway, Suite 1204, Arlington, VA 22202-4302. Respondents should be aware that notwithstanding any other provision of law, no person shall be subject to any penalty for failing to comply with a collection of information if it does not display a currently valid OMB control number. **PLEASE DO NOT RETURN YOUR FORM TO THE ABOVE ADDRESS**.

1. REPORT DATE *(DD-MM-YY)*	2. REPORT TYPE	3. DATES COVERED *(From - To)*
August 2012	Technical Paper	1 July 2012 – 1 August 2012

4. TITLE AND SUBTITLE
POROSITY EVOLUTION IN A CREEPING SINGLE CRYSTAL (PREPRINT)

5a. CONTRACT NUMBER
FA8650-08-C-5226

5b. GRANT NUMBER

5c. PROGRAM ELEMENT NUMBER
62102F

6. AUTHOR(S)
A. Srivastava and A. Needleman

5d. PROJECT NUMBER
4347

5e. TASK NUMBER

5f. WORK UNIT NUMBER
LM114100

7. PERFORMING ORGANIZATION NAME(S) AND ADDRESS(ES)
University of North Texas
Corner of Avenue C Chestnut
Denton, TX 76203

8. PERFORMING ORGANIZATION REPORT NUMBER

9. SPONSORING/MONITORING AGENCY NAME(S) AND ADDRESS(ES)
Air Force Research Laboratory
Materials and Manufacturing Directorate
Wright-Patterson Air Force Base, OH 45433-7750
Air Force Materiel Command
United States Air Force

10. SPONSORING/MONITORING AGENCY ACRONYM(S)
AFRL/RXCM

11. SPONSORING/MONITORING AGENCY REPORT NUMBER(S)
AFRL-RX-WP-TP-2012-0373

12. DISTRIBUTION/AVAILABILITY STATEMENT
Approved for public release; distribution unlimited. Preprint to be submitted to MSMSE.

13. SUPPLEMENTARY NOTES
The U.S. Government is joint author of this work and has the right to use, modify, reproduce, release, perform, display, or disclose the work. PA Case Number and clearance date: 88ABW-2012-2170, 11 April 2012. This document contains color.

14. ABSTRACT
Experimental observations on tensile specimens in [1] indicated that the growth of initially present processing induced voids in a nickel based single crystal superalloy played a significant role in limiting creep life. Also, creep tests on single crystal superalloy specimens typically show greater creep strain rates and/or reduced creep life for thinner specimens than predicted by current theories. In order to quantify the role of void growth in single crystals in creep loading, we have carried out three dimensional finite deformation finite element analyses of unit cells containing a single initially spherical void. The materials are characterized by a rate dependent crystal plasticity constitutive relation accounting for primary and secondary creep. Two types of imposed loading are considered: an applied true stress (force/unit current area) that is time independent; and an applied nominal stress (force/unit initial area) that is time independent. Isothermal conditions are assumed. The evolution of porosity is calculated for various values of stress triaxiality and of the Lode parameter. The evolution of porosity with time is sensitive to whether constant true stress or constant...

15. SUBJECT TERMS
creep, superalloy, crystal plasticity, void growth, void collapse, Lode parameter, finite elements

16. SECURITY CLASSIFICATION OF:			17. LIMITATION OF ABSTRACT:	NUMBER OF PAGES	19a. NAME OF RESPONSIBLE PERSON (Monitor)
a. REPORT	b. ABSTRACT	c. THIS PAGE			Jaimie Tiley
Unclassified	Unclassified	Unclassified	SAR	26	19b. TELEPHONE NUMBER *(Include Area Code)* N/A

Porosity Evolution in a Creeping Single Crystal

A. Srivastava, A. Needleman

Department of Materials Science and Engineering, College of Engineering, University of North Texas, Denton, TX

Abstract. Experimental observations on tensile specimens in [1] indicated that the growth of initially present processing induced voids in a nickel based single crystal superalloy played a significant role in limiting creep life. Also, creep tests on single crystal superalloy specimens typically show greater creep strain rates and/or reduced creep life for thinner specimens than predicted by current theories. In order to quantify the role of void growth in single crystals in creep loading, we have carried out three dimensional finite deformation finite element analyses of unit cells containing a single initially spherical void. The materials are characterized by a rate dependent crystal plasticity constitutive relation accounting for primary and secondary creep. Two types of imposed loading are considered: an applied true stress (force/unit current area) that is time independent; and an applied nominal stress (force/unit initial area) that is time independent. Isothermal conditions are assumed. The evolution of porosity is calculated for various values of stress triaxiality and of the Lode parameter. The evolution of porosity with time is sensitive to whether constant true stress or constant nominal stress loading is applied. However, the evolution of porosity with the overall unit cell strain is insensitive to the mode of loading. At high values of stress triaxiality, the response is essentially independent of the value of the Lode parameter. At sufficiently low values of the stress triaxiality, the porosity evolution depends on the value of the Lode parameter and void collapse can occur. Also, rather large stress concentrations can develop which could play a role in the observed thickness dependence.

Keywords: creep, superalloy, crystal plasticity, void growth, void collapse, Lode parameter, finite elements.

1. Introduction

The motivation for this study stems from experimental observations of creep deformation and failure of a nickel based single crystal superalloy, [1, 2]. Metallographic observations have shown that Ni-based single crystal superalloys contain micro voids formed during the solidification and homogenization processes [1,3,4]. A variety of experimental results, e.g. [2,5,6], have shown greater creep strain rates and reduced creep life for thinner specimens (but still larger than the micron scale at which size dependent plasticity effects come into play) than is predicted by current theories. This is termed the thickness debit effect and is typically attributed to some sort of surface damage as in [7–9]. Isothermal creep tests carried out on plate-like specimens of a PWA1484 nickel-based single crystal superalloy having various thicknesses and deformed at several stress levels and temperatures in [1,2] showed a thickness debit effect even at temperatures too low for there to be any significant effect of diffusion or environmental damage. Void growth was observed in [1] and played a role in the creep failure process.

Here, we analyze void growth in a single crystal matrix using a unit cell model. Each unit cell contains a single initially spherical void. Isothermal conditions are assumed and we confine attention to circumstances where diffusion effects have a negligible influence on void growth. Finite deformation finite element analyses are carried out using a rate dependent crystal plasticity constitutive relation accounting

Approved for public release; distribution unlimited.

for both primary and secondary creep. We consider one initial crystallographic orientation, that in the experiments in [1, 2], and one initial void volume fraction.

There is a large literature on cell models of porosity evolution aimed at understanding the micromechanics of ductile fracture and developing damage-type constitutive relations, e.g. [10–21]. The initial focus was on relatively high values of stress triaxiality where the effect of the stress triaxiality (the ratio of the first and second stress invariants) is dominant, for example [10–17]. More recently, largely motivated by experiments of Bao and Wierzbicki [22], modeling the behavior at moderate and low values of stress triaxiality where the influence of the third stress invariant becomes more prominent has been receiving much attention, e.g. [18–21]. These studies have been carried out for isotropic solids and for imposed loadings where the applied stress increases with time.

Hori and Nemat-Nasser [23] analyzed void growth and void collapse in a three dimensional single crystal matrix with an isolated ellipsoidal void under far field tensile and compressive loading. Void growth in two dimensional single crystals have been analyzed in [24–27]. Kysar et al. [27] used anisotropic slip line theory to obtain stress and deformation state around a cylindrical void in a single crystal oriented such that plane strain conditions are admitted from three effective in-plane slip systems. Void growth in a single crystal was analyzed in [28–35] using a three dimensional cell model based crystal plasticity calculation that accounts for void-void interaction effects. Wan et al. [29] and Yu et al. [35] analyzed the effect of the Lode parameter (a parameter that characterizes the third invariant of stress) on void growth. It has been shown that the effect of the Lode parameter can depend on crystallographic orientation [35] and void shape (crack-like or pore-like) [30]. All these results were obtained for monotonically increasing loading conditions.

For creep loading, Budiansky et al. [36] analyzed deformation of an isolated void in an isotropic viscous material under a wide range of remote axisymmetric stress states. Based on the void growth model in [36], Dennis [37] (also see [38]) carried out an analysis of an isolated void in a single crystal and proposed a failure criterion for the initiation of a microcrack from a void surface in terms of a critical inelastic strain in the vicinity of the void which in turn was linked to a stress triaxiality dependent critical relative void volume fraction. Finite deformation analyses of the effect of void interaction and void shape change on the void growth rate in an isotropic power law creeping matrix were carried out in [39]. For polycrystalline metals, grain boundary diffusion often plays a significant role, see for example [40, 41]. However, for single crystals this mechanism is ruled out and, at least for one of the temperatures tested in [1, 2], 760°C, bulk diffusion also was not significant so that dislocation creep was the main deformation mechanism.

Our analyses focus on the role of stress state on deformation and void growth in ductile single crystals in the dislocation creep regime. We also explore the possible role of porosity evolution in the thickness debit effect. We consider two types of imposed loading: in one case the applied true stress (force/current area) is fixed in time while in the other case the applied nominal stress (force/initial area) is time independent. For both type of loading we analyze stress states corresponding to various values of triaxiality (the ratio of hydrostatic to Mises effective stress) and various values of the Lode parameter. The true stress conditions are of interest for constitutive modeling while the experiments in [1, 2] were carried out under fixed nominal stress loading conditions. Results are presented for the effects of stress triaxiality and Lode parameter on the evolution of the void volume fraction and the void shape as well as for the effect of void shape changes on the stress state that develops in the crystal matrix.

2. Problem Formulation

2.1. Unit cell

We carry out three dimensional cell model analyses of a single initially spherical void in a face centered cubic (fcc) crystal under tensile creep loading conditions. Cartesian tensor notation is used. The unit cell is initially cubic with side lengths $2a_0$ ($-a_0 \leq x_i \leq a_0$) and the initial void radius is r_0. The main loading

Approved for public release; distribution unlimited.

direction is parallel to the x_1 axis and the edges initially parallel to the x_2 and x_3 axes are required to remain parallel to their respective axes during deformation which is consistent with, but stronger than, symmetry about these axes. The fcc crystal is taken to be in a $< 001 >$ (cube) orientation. Symmetry about each axis is assumed so that only 1/8 of the unit cell needs to be analyzed numerically. The configuration analyzed is shown in Fig. 1.

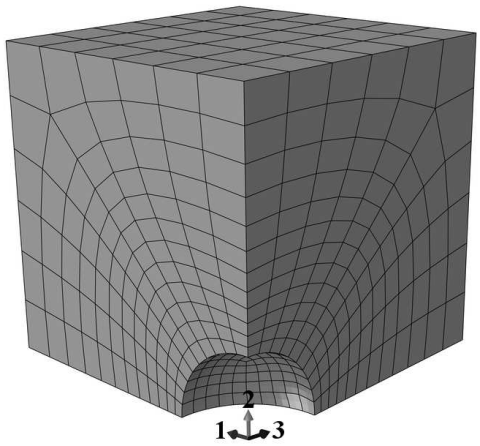

Figure 1. A finite element mesh of 1/8 of the unit cell with a spherical void in the center.

Overall tractions are imposed on the faces of the unit cell with the requirement that the cell boundaries remain planes aligned with the coordinate axes and shear free so that

$$\begin{aligned} &u_1(a_0, x_2, x_3) = U_1(t)\ ,\ T_2(a_0, x_2, x_3) = 0\ ,\ T_3(a_0, x_2, x_3) = 0 \\ &u_2(x_1, a_0, x_3) = U_2(t)\ ,\ T_1(x_1, a_0\, x_3) = 0\ ,\ T_3(x_1, a_0, x_3) = 0 \\ &u_3(x_1, x_2, a_0) = U_3(t)\ ,\ T_1(x_1, x_2, a_0) = 0\ ,\ T_2(x_1, x_2, a_0) = 0 \end{aligned} \tag{1}$$

The symmetry conditions on the remaining surfaces are

$$\begin{aligned} &u_1(0, x_2, x_3) = 0\ ,\ T_2(0, x_2, x_3) = 0\ ,\ T_3(0, x_2, x_3) = 0 \\ &u_2(x_1, 0, x_3) = 0\ ,\ T_1(x_1, 0, x_3) = 0\ ,\ T_3(x_1, 0, x_3) = 0 \\ &u_3(x_1, x_2, 0) = 0\ ,\ T_1(x_1, x_2, 0) = 0\ ,\ T_2(x_1, x_2, 0) = 0 \end{aligned} \tag{2}$$

The macroscopic true (or Cauchy) stresses, Σ_i, are defined as

$$\begin{aligned} \Sigma_1 &= \frac{1}{a_2 a_3} \int_0^{a_2} \int_0^{a_3} \sigma_{11}(a_1, x_2, x_3) dx_2 dx_3 \\ \Sigma_2 &= \frac{1}{a_1 a_3} \int_0^{a_1} \int_0^{a_3} \sigma_{22}(x_1, a_2, x_3) dx_1 dx_3 \\ \Sigma_3 &= \frac{1}{a_1 a_2} \int_0^{a_1} \int_0^{a_2} \sigma_{33}(x_1, x_2, a_3) dx_1 dx_2 \end{aligned} \tag{3}$$

where $a_1 = a_0 + U_1$, $a_2 = a_0 + U_2$ and $a_3 = a_0 + U_3$.

The time histories of the displacements $U_1(t)$, $U_2(t)$ and $U_3(t)$ in Eq. (1) are determined by the analysis. In one set of calculations, true stresses Σ_1, Σ_2 and Σ_3 are applied and remain constant throughout the deformation history. In the other set of calculations, the value of the nominal (or engineering) stress, N_1 is required to remain fixed throughout the deformation history. The macroscopic nominal stress N_i are related to the values of Σ_i in Eq. (3) by

$$N_1 = \frac{a_2 a_3}{a_0^2} \Sigma_1\ ,\ N_2 = \frac{a_1 a_3}{a_0^2} \Sigma_2\ ,\ N_3 = \frac{a_1 a_2}{a_0^2} \Sigma_3 \tag{4}$$

Approved for public release; distribution unlimited.

For both types of imposed loading, the macroscopic true stresses follow a proportional stress history that is given by

$$\Sigma_2 = \rho_2 \Sigma_1 \qquad \Sigma_3 = \rho_3 \Sigma_1 \tag{5}$$

where ρ_2 and ρ_3 are constants. Hence, with N_1 fixed and proportional true stress values imposed N_2 and N_3 generally vary during the loading history. However, for uniaxial tensile loading $\Sigma_2 = \Sigma_3 = 0$, the values of N_2 and N_3 also remain zero. Here, calculations with Σ_1 fixed (and by Eq. (5) Σ_2 and Σ_3 fixed) are termed constant true stress calculations while calculations with N_1 fixed are termed constant nominal stress calculations even though N_2 and N_3 typically vary during the deformation history.

The macroscopic effective stress, Σ_e, and the macroscopic hydrostatic stress (positive in tension), Σ_h, are given by

$$\Sigma_e = \frac{1}{\sqrt{2}} \sqrt{(\Sigma_1 - \Sigma_2)^2 + (\Sigma_2 - \Sigma_3)^2 + (\Sigma_3 - \Sigma_1)^2} \qquad \Sigma_h = \frac{1}{3}(\Sigma_1 + \Sigma_2 + \Sigma_3) \tag{6}$$

The stress triaxiality χ, is then defined as

$$\chi = \frac{\Sigma_h}{\Sigma_e} = \frac{\sqrt{2}}{3} \frac{1 + \rho_2 + \rho_3}{\sqrt{(1 - \rho_2)^2 + (\rho_2 - \rho_3)^2 + (\rho_3 - 1)^2}} \tag{7}$$

The stress triaxiality involves the first and second stress invariants, the influence of the third invariant is assessed via the Lode parameter, L, which is

$$L = \frac{2\Sigma_2 - \Sigma_1 - \Sigma_3}{\Sigma_1 - \Sigma_3} = \frac{2\rho_2 - 1 - \rho_3}{1 - \rho_3} \tag{8}$$

2.2. Constitutive relation

The crystal plasticity constitutive implementation is based on the UMAT due to Huang [42] as modified by Kysar [43]. This crystal constitutive formulation follows that in Asaro and Needleman [44] (see also Asaro [45]). The deformation gradient, $\mathbf{F}$, is written as

$$\mathbf{F} = \mathbf{F}^* \cdot \mathbf{F}^P \tag{9}$$

where $\mathbf{F}^*$ is due to stretching and rotation of the crystal lattice and $\mathbf{F}^P$ is due to crystallographic slip. In the reference, undeformed lattice, the slip direction and the slip plane normals of the crystal are denoted by $\mathbf{s}^{(\alpha)}$ and $\mathbf{m}^{(\alpha)}$, respectively. In the current configuration these are given by

$$\mathbf{s}^{(\alpha)*} = \mathbf{F}^* \cdot \mathbf{s}^{(\alpha)} \qquad \mathbf{m}^{(\alpha)*} = \mathbf{m}^{(\alpha)} \cdot \mathbf{F}^{*-1} \tag{10}$$

Differentiating Eq. (9) with respect to time and combining terms gives

$$\dot{\mathbf{F}} \cdot \mathbf{F}^{-1} = \mathbf{D} + \mathbf{\Omega} = (\mathbf{D}^* + \mathbf{\Omega}^*) + (\mathbf{D}^p + \mathbf{\Omega}^p) \tag{11}$$

Here, $(\mathbf{D}^* + \mathbf{\Omega}^*)$ are, respectively, the elastic rate of stretching and spin tensors, and the plastic rate of stretching, $\mathbf{D}^p$, and spin tensors, $\mathbf{\Omega}^p$, are given by

$$\mathbf{D}^p = \sum_\alpha \dot{\gamma}^{(\alpha)} \mathbf{P}^{(\alpha)} \qquad \mathbf{\Omega}^p = \sum_\alpha \dot{\gamma}^{(\alpha)} \mathbf{W}^{(\alpha)} \tag{12}$$

where $\dot{\gamma}^{(\alpha)}$ is the rate of shearing on slip system α, and

$$\mathbf{P}^{(\alpha)} = \frac{1}{2}(\mathbf{s}^{(\alpha)*}\mathbf{m}^{(\alpha)*} + \mathbf{m}^{(\alpha)*}\mathbf{s}^{(\alpha)*}) \qquad \mathbf{W}^{(\alpha)} = \frac{1}{2}(\mathbf{s}^{(\alpha)*}\mathbf{m}^{(\alpha)*} - \mathbf{m}^{(\alpha)*}\mathbf{s}^{(\alpha)*}) \tag{13}$$

Elastic strains are presumed small so that the lattice Jaumann rate of Cauchy stress, $\hat{\boldsymbol{\sigma}}^*$, is given by

$$\hat{\boldsymbol{\sigma}}^* = \dot{\boldsymbol{\sigma}} + \boldsymbol{\sigma} \cdot \mathbf{\Omega}^* - \mathbf{\Omega}^* \cdot \boldsymbol{\sigma} = \mathbf{L} : \mathbf{D}^* - \boldsymbol{\sigma}(\mathbf{I} : \mathbf{D}^*) \tag{14}$$

with $\mathbf{L}$ being the tensor of elastic moduli. The corotational stress rate on axes rotating with the material, $\hat{\boldsymbol{\sigma}}$, is given by

$$\hat{\boldsymbol{\sigma}} = \dot{\boldsymbol{\sigma}} - \mathbf{\Omega} \cdot \boldsymbol{\sigma} + \boldsymbol{\sigma} \cdot \mathbf{\Omega} \tag{15}$$

Approved for public release; distribution unlimited.

The difference between $\hat{\boldsymbol{\sigma}}^*$ and $\hat{\boldsymbol{\sigma}}$ is

$$\hat{\boldsymbol{\sigma}}^* - \hat{\boldsymbol{\sigma}} = \sum_\alpha \dot{\gamma}^{(\alpha)} \mathbf{W}^{(\alpha)} \cdot \boldsymbol{\sigma} - \sum_\alpha \dot{\gamma}^{(\alpha)} \boldsymbol{\sigma} \cdot \mathbf{W}^{(\alpha)} \tag{16}$$

Defining

$$\boldsymbol{\psi}^{(\alpha)} = \mathbf{W}^{(\alpha)} \cdot \boldsymbol{\sigma} - \boldsymbol{\sigma} \cdot \mathbf{W}^{(\alpha)} \tag{17}$$

and using Eqs. (11) and (12) with Eqs. (14) and (16) gives

$$\hat{\boldsymbol{\sigma}} = (\mathbf{L} - \boldsymbol{\sigma}\mathbf{I}) : \mathbf{D} - \sum_\alpha \dot{\gamma}^{(\alpha)} \mathbf{R}^{(\alpha)} \tag{18}$$

since $\mathbf{I} : \mathbf{D}^* = \mathbf{I} : \mathbf{D}$ and with

$$\mathbf{R}^{(\alpha)} = \mathbf{L} : \mathbf{P}^{(\alpha)} + \boldsymbol{\psi}^{(\alpha)} \tag{19}$$

The Schmid resolved shear stress is given by

$$\tau^{(\alpha)} = \mathbf{m}^{(\alpha)*} \cdot \boldsymbol{\sigma} \cdot \mathbf{s}^{(\alpha)*} = \boldsymbol{\sigma} : \mathbf{P}^{(\alpha)} \tag{20}$$

The material modeled is a PWA1484 Ni based single crystal superalloy [2]. The elastic constants have cubic symmetry and are specified by $C_{11} = 283.3$GPa, $C_{12} = 197.5$GPa and $C_{44} = 112$GPa. The active slip systems for this material at the temperature of interest are not known. Given the fcc-based crystal structure, we take the potentially active slip system to be the twelve primary octahedral slip systems $\{111\} < 110 >$.

Slip is assumed to obey Schmid's law so that the slip rate $\dot{\gamma}^{(\alpha)}$ only depends on the current stress state through the slip-system resolved shear stress $\tau^{(\alpha)}$. The crystals exhibit both primary and secondary creep, both of which are represented in terms of power law relations. The initial value of slip on each slip system is taken to be zero and the evolution of slip on slip system α is given by

$$\dot{\gamma}^{(\alpha)} = \left\{ (1-\beta)\dot{\gamma}_M \left| \frac{\tau^{(\alpha)}}{\tau_0} \right|^M + \beta \dot{\gamma}_N \left| \frac{\tau^{(\alpha)}}{\tau_0} \right|^N \right\} \mathrm{sgn}(\tau) \tag{21}$$

where τ_0, $\dot{\gamma}_M$, $\dot{\gamma}_N$, M and N are material constants and β evolves as

$$\dot{\beta} = \frac{1}{t_0} (\beta_{ss} - \beta) \tag{22}$$

with the initial condition that $\beta = 0$ at $t = 0$ and with β_{ss} the steady state value of β and t_0 a time constant that governs the transition from primary to secondary creep. This particular form was fit to the experimental constant applied nominal stress creep data of Seetharaman and Cetel [2] for the sheet specimen of thickness 3.18mm at a test temperature of 760°C and an applied nominal stress of $N_1 = 758$MPa. The material parameters used in Eq. (21) are $\tau_0 = 245$MPa, $\dot{\gamma}_M = 1.04 \times 10^{-6}\mathrm{s}^{-1}$, $\dot{\gamma}_N = 1.53 \times 10^{-9}\mathrm{s}^{-1}$, $M = 1$ and $N = 5$ and the parameters used in Eq. (22) are $\beta_{ss} = 0.998$ and $t_0 = 1.35 \times 10^4$s. Figure 2 shows the experimental tensile creep curve of $\Delta l/l_0$ versus time, where l_0 is the initial length of the specimen gauge section and Δl is the change in length of the gauge section with the loading applied in the $< 001 >$ direction. For comparison purposes two computed curves for a fully dense material using the parameter values given above are also plotted: one with constant nominal stress and one with constant true stress. The computed and experimental curves with a constant nominal stress are in good agreement until the time at which the onset of tertiary creep occurs in the experiment.

Approved for public release; distribution unlimited.

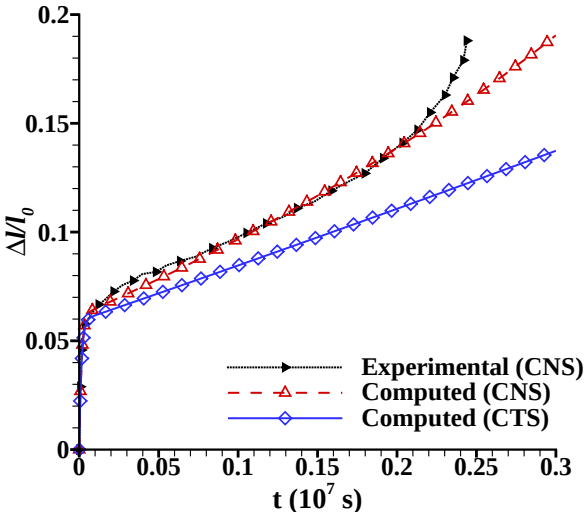

Figure 2. Comparison of experimental and computed tensile creep curves for a single crystal of orientation $< 001 >$. The experimental creep curve is obtained for constant nominal stress creep loading and the computed creep curves are shown for both constant nominal stress (CNS) and constant true stress (CTS) creep loading. The computed curves are for a fully dense material.

2.3. Numerical method

The calculations are carried out using the commercial finite element code ABAQUS standard, version 6.x [46], and using a UMAT based on that developed by Huang [42] and Kysar [43] modified for the creep relation in Section 2.2. In all calculations the initial values of Σ_i are prescribed so that $\Sigma_1 \geq \Sigma_2 \geq \Sigma_3$. In the calculations with fixed values of the true stresses Σ_i the values of the stress triaxiality χ and the Lode parameter L directly remain fixed. In the calculations with the nominal stress N_1 kept fixed the values of Σ_i vary with time so that the fixed stress ratio in Eq. (5) needs to be maintained by controlling the tractions acting on the surfaces of the unit cell. At each time step the values of Σ_i are calculated from Eq. (3). The proportional history of stress state is monitored using the URDFIL user subroutine in ABAQUS standard 6.x [46] and any deviation in the proportionality constants ρ_2 and ρ_3 given in Eq. (5) is counteracted by applying an additional uniform traction on the corresponding surfaces using the DLOAD user subroutine. The variations in ρ_2 and ρ_3 were kept within 0.1% over the course of the loading history. This procedure enables the responses under prescribed true stress conditions and under prescribed nominal stress N_1 to be compared for fixed χ and L values. Prescribed proportional true stressing is of interest for formulating a phenomenological damage-type constitutive relation while the interest in prescribed nominal stressing is because that is the condition in the creep experiments in [1, 2].

A finite element mesh with C3D20H (20-node hybrid solid elements with quadratic displacement interpolation and linear pressure interpolation) elements is shown in Fig. 1. Most calculations are carried out using 916 elements. Convergence was assessed by carrying out calculations with 1250 and 1786 elements for a representative case with $\chi = 2$, $L = -1$ and fixed Σ_i. The time to reach an effective creep strain of $E_e = 0.3$ was used to assess convergence. For meshes with 916, 1250 and 1786 elements the time to $E_e = 0.3$ was 7.2889×10^6s, 7.2887×10^6s and 7.2885×10^6s respectively. The time steps were varied during the course of the deformation history so that $\Delta\gamma^{(\alpha)}$ on any slip system never exceeded 0.001.

Approved for public release; distribution unlimited.

3. Numerical Results

The unit cell analyzed, see Fig. 1, has $r_0/a_0 = 0.267$ which gives a void volume fraction of $(4\pi r_0^3/3)/(2a_0)^3 = 0.01$. This is selected based on the distribution of porosity in the material in [1]. The average void volume fraction in a Ni-based single crystal material is generally low but these pores are confined in interdendritic areas [3,4], hence leading to a higher local void volume fraction. This initial void volume fraction and the crystal properties are the same in all calculations. The loading axis in the creep tests of [2] is within 10° of $< 001 >$ and $< 001 >$ tensile loading is prescribed in the calculations here.

In the first time step values of Σ_i are specified that give a value of Σ_e in Eq. (6) of 750MPa and the crystal response is taken to be elastic. Calculations are carried out for six values of the stress triaxiality χ, Eq. (7), and, for each value of χ, for five values of the Lode parameter L, Eq. (8). The stress state is taken to be such that $\Sigma_1 \geq \Sigma_2 \geq \Sigma_3$. The expressions Eq. (7) and Eq. (8) together with $\Sigma_e = 750$MPa in Eq. (6) constitute a set of quadratic equations for the stress components. For a given value of χ and L two sets of values of the stress components are obtained only one of which satisfies the specified inequality constraint. For example, with $\chi = 3$ and $L = -1$ the two solutions are: $\Sigma_1 = 2750$MPa, $\Sigma_2 = 2000$MPa, $\Sigma_3 = 2000$MPa; and $\Sigma_1 = 1750$MPa, $\Sigma_2 = 2500$MPa, $\Sigma_3 = 2500$MPa. A reordering of the second of these solutions to $\Sigma_1 = 2500$MPa, $\Sigma_2 = 2500$MPa, $\Sigma_3 = 1750$MPa corresponds to $\chi = 3$, $L = 1$. Similarly for other combinations of χ and L, the solution that does not satisfy the inequality constraint gives stress components with the same value of χ and a sign change in L when the stresses are reordered.

The initial stress states together with the values of stress triaxiality χ, the Lode parameter L and the parameter ω introduced by Nahshon and Hutchinson [20] are shown in Table. 1. The value of ω is given by

$$\omega = 1 - \left(\frac{27 J_3}{2\Sigma_e^3}\right)^2 \tag{23}$$

where, $J_3 = (\Sigma_1 - \Sigma_h)(\Sigma_2 - \Sigma_h)(\Sigma_3 - \Sigma_h)$ with Σ_e and Σ_h defined in Eq. (6).

For each initial stress state, the creep response under both constant true stress and constant nominal stress loading is analyzed. For constant true stress creep Σ_i remains constant through out loading history whereas for constant nominal stress creep Σ_i varies during the deformation history.

The parameter ω defined in [20], lies in the range $0 \leq \omega \leq 1$, with $\omega = 0$ for all axisymmetric stress states and $\omega = 1$ for all stress comprised of a pure shear stress plus a hydrostatic contribution. Thus, ω does not distinguish between the imposed stress states corresponding to $L = -1$ and $L = 1$. In the following we use the Lode parameter L to characterize the imposed stress state.

The macroscopic effective creep strain is defined as

$$E_e = \frac{\sqrt{2}}{3}\sqrt{(E_1^c - E_2^c)^2 + (E_2^c - E_3^c)^2 + (E_3^c - E_1^c)^2} \tag{24}$$

where

$$E_1^c = \ln\left(\frac{a_1}{\tilde{a}_1}\right) \qquad E_2^c = \ln\left(\frac{a_2}{\tilde{a}_2}\right) \qquad E_3^c = \ln\left(\frac{a_3^c}{\tilde{a}_3}\right) \tag{25}$$

where $\tilde{a}_i$ is the value of a_i after the first elastic step.

The calculations proceed with fixed true or nominal stresses until one of the following conditions is met: (i) 90% loss of ligament in either the x_2 or the x_3 direction; (ii) void collapse, $f/f_0 \approx 0$; or (iii) achieving an effective macroscopic creep strain $E_e = 1.5$.

3.1. Evolution of the macroscopic creep strain

The time history of E_e for stress triaxiality values $\chi = 3$ and 0.33 and values of the Lode parameter ranging from -1 to 1 is shown in Fig. 3 under constant true stress creep loading conditions. The transition from

Approved for public release; distribution unlimited.

Table 1. Initial values of the stress triaxiality χ, the Lode parameter L, the parameter ω and the initial macroscopic stresses Σ_i.

χ	L	ω	Σ_1 (MPa)	Σ_2 (MPa)	Σ_3 (MPa)
3.00	-1.00	0.00	2750.00	2000.00	2000.00
3.00	-0.50	0.44	2735.36	2111.33	1903.31
3.00	0.00	1.00	2683.01	2250.00	1816.99
3.00	0.50	0.44	2596.69	2388.68	1764.64
3.00	1.00	0.00	2500.00	2500.00	1750.00
2.00	-1.00	0.00	2000.00	1250.00	1250.00
2.00	-0.50	0.44	1985.36	1361.33	1153.31
2.00	0.00	1.00	1933.01	1500.00	1066.99
2.00	0.50	0.44	1846.69	1638.68	1014.64
2.00	1.00	0.00	1750.00	1750.00	1000.00
1.00	-1.00	0.00	1250.00	500.00	500.00
1.00	-0.50	0.44	1235.36	611.32	403.31
1.00	0.00	1.00	1183.01	750.00	316.99
1.00	0.50	0.44	1096.69	888.68	264.64
1.00	1.00	0.00	1000.00	1000.00	250.00
0.75	-1.00	0.00	1062.50	312.50	312.50
0.75	-0.50	0.44	1047.86	423.82	215.81
0.75	0.00	1.00	995.51	562.50	129.49
0.75	0.50	0.44	909.19	701.18	77.14
0.75	1.00	0.00	812.50	812.50	62.50
0.50	-1.00	0.00	875.00	125.00	125.00
0.50	-0.50	0.44	860.36	236.32	28.31
0.50	0.00	1.00	808.01	375.00	-58.01
0.50	0.50	0.44	721.69	513.68	-110.36
0.50	1.00	0.00	625.00	625.00	-125.00
0.33	-1.00	0.00	750.00	0.00	0.00
0.33	-0.50	0.44	735.36	111.32	-96.69
0.33	0.00	1.00	683.01	250.00	-183.01
0.33	0.50	0.44	596.69	388.68	-235.36
0.33	1.00	0.00	500.00	500.00	-250.00

primary to secondary (steady state) creep, governed by the evolution of β in Eq. (22), is essentially independent of the stress triaxiality and occurs at $t \approx 1.0 \times 10^5$s. This corresponds to $E_e = 0.061$ for $\chi = 3$ and $L = -1$ and to $E_e = 0.058$ for $\chi = 0.33$ and $L = -1$. The steady state effective creep strain rate, $\dot{E}_{ss}$, is essentially independent of the value of the Lode parameter and is almost same for $\chi \leq 0.75$ as for the fully dense material in Fig. 2 which is $\dot{E}_{ss} = 0.235 \times 10^{-7}\text{s}^{-1}$. For greater values of the stress triaxiality χ there is an effect of χ on $\dot{E}_{ss}$ with $\dot{E}_{ss}$ increasing to $\dot{E}_{ss} = 0.438 \times 10^{-7}\text{s}^{-1}$ for $\chi = 3$.

For $\chi = 3$, Fig. 3(a), there is a transition to tertiary creep which, as will be shown subsequently, is associated with necking of the ligament between adjacent voids. Under the creep loading conditions here the increase in strain rate accompanying necking occurs less abruptly than for the nearly rate independent materials in [13]. Here, and subsequently, we will identify the time at which tertiary creep begins as the earliest time at which $\dot{E}_e/\dot{E}_{ss} \geq 5$. With this definition, in Fig. 3(a) where $\chi = 3$ the onset of tertiary creep occurs at $t \approx 0.32 \times 10^7$s. For $\chi = 0.33$, Fig. 3(b), tertiary creep does not occur over the range

Approved for public release; distribution unlimited.

computed and the calculations are terminated either when void collapse occurs or when $E_e = 1.5$. The maximum quantitative difference in Fig. 3(b) is between the curves for $L = \pm 1$ and $L = 0$.

The values $L = -1$ and $L = 1$ both correspond to axisymmetric stress states. For a fully dense single crystal, the number of slip systems with the same magnitude of resolved shear stress is the same and the number of systems with positive and negative values of resolved shear stress are also the same although the particular slip systems differ. For example, with $\chi = 0.33$, there are four slip systems with $\tau = 306.3$MPa and four with $\tau = -306.3$MPa for both $L = 1$ and $L = -1$. Nevertheless, the responses with a void differ with different values of Lode parameter in particular at low values of stress triaxiality.

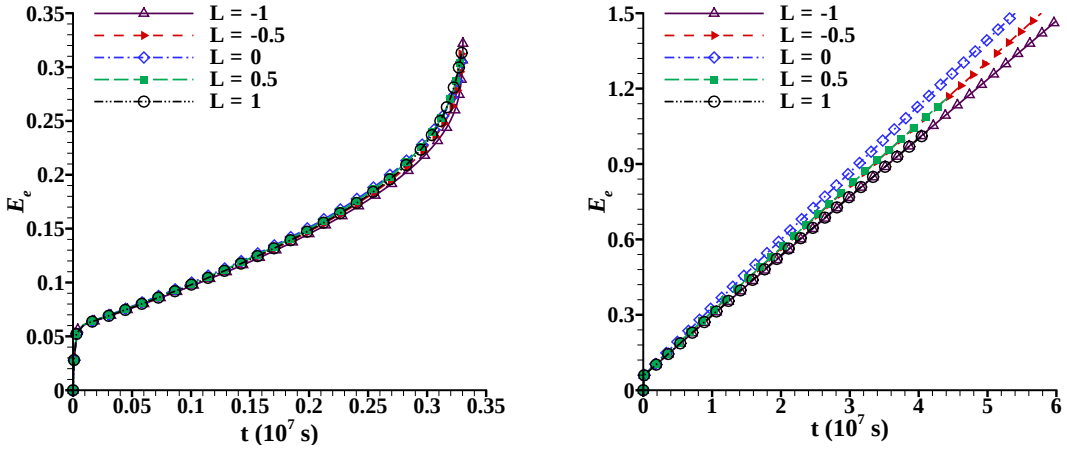

(a) Stress triaxiality $\chi = 3$ (b) Stress triaxiality $\chi = 0.33$

Figure 3. Time histories of macroscopic effective creep strain E_e under constant true stress creep loading for stress triaxiality (a) $\chi = 3$ and (b) $\chi = 0.33$.

The variation of macroscopic effective strain, E_e, with time for all six values of stress triaxiality, χ, is shown in Fig. 4 for $L = -1$ and $L = 1$. Whether or not tertiary creep occurs depends on the value of the stress triaxiality, χ, and, if it does occur, the value of time at which it occurs also depends on the value of χ. For $L = -1$ to $L = 1$ tertiary creep (as defined here) occurs for $\chi \geq 2$ and does not occur for $\chi \leq 0.75$. The value of χ at which the transition from tertiary creep occurring to no tertiary creep (over the time computed) does depend on the value of the Lode parameter L. For example, tertiary creep occurs for $\chi = 1$ and $L = -1$ at $t = 3.5 \times 10^7$s but for $\chi = 1$ and $L = 1$, $\dot{E}_e/\dot{E}_{ss}$ remains less than 5 till 90% loss of ligament. The curves for $\chi = 0.5$ and $\chi = 0.33$ with $L = 1$ in Fig. 4(b) are terminated before $E_e = 1.5$ because void collapse occurred as will be shown in Section 3.2.

The results for constant nominal stress creep loading are shown in Figs. 5 and 6. Under constant nominal stress creep loading, Σ_1 increases with the deformation induced reduction in cross sectional area perpendicular to the x_1 direction, see Eq. (4). In contrast to the results for constant true stress creep loading, there is a significant dependence on the value of the Lode parameter L for all values of χ in Fig. 5. In particular, the responses for $L = -1$ and $L = 1$ differ significantly. The steady state effective strain rate for a fully dense material with constant N_1 in Fig. 2 is $\dot{E}_{ss} = 0.355 \times 10^{-7} s^{-1}$. There is a small effect of porosity (with $f_0 = 0.01$) on the steady state creep rate for $\chi = 0.33$; $\dot{E}_{ss} = 0.395 \times 10^{-7}\text{s}^{-1}$ for $\chi = 0.33$ and $L = -1$. As for constant Σ_i loading, the effect of porosity on the secondary creep rate increases with increasing stress triaxiality being $0.61 \times 10^{-7}\text{s}^{-1}$ for $\chi = 3$ and $L = -1$. At all values of χ, the effect of porosity is greater under constant N_1 (nominal stress) loading than it is under constant Σ_i (true stress) loading.

Approved for public release; distribution unlimited.

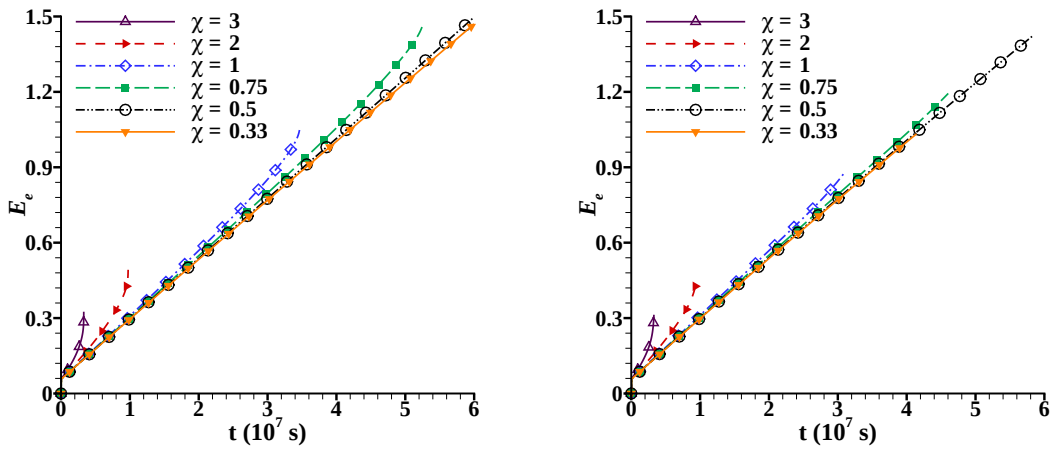

(a) Lode parameter $L = -1$ (b) Lode parameter $L = 1$

Figure 4. Time histories of macroscopic effective creep strain E_e under constant true stress creep loading for Lode parameter (a) $L = -1$ and (b) $L = 1$.

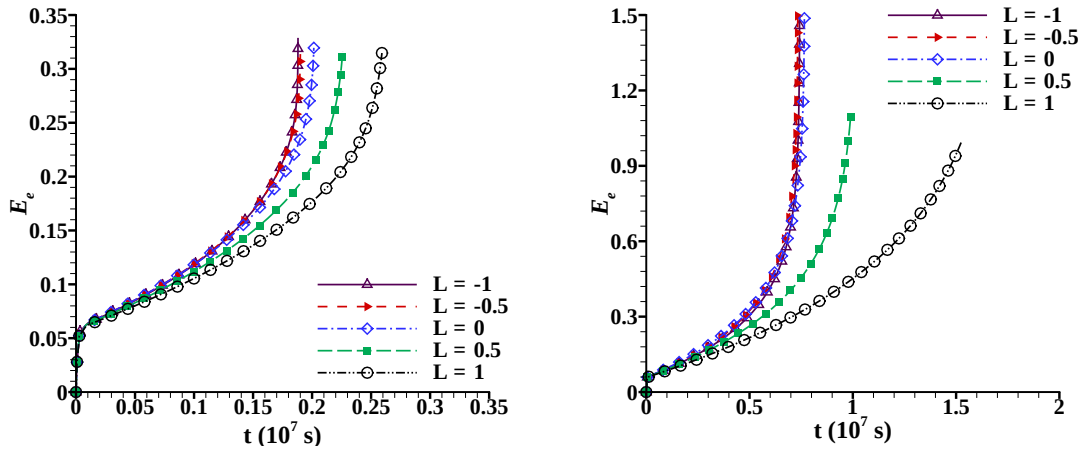

(a) Stress triaxiality $\chi = 3$ (b) Stress triaxiality $\chi = 0.33$

Figure 5. Time histories of macroscopic effective creep strain E_e for constant nominal stress creep loading for stress triaxiality (a) $\chi = 3$ and (b) $\chi = 0.33$.

Under constant nominal stress loading, tertiary creep occurs for $\chi = 0.33$. and there is a significant dependence on the values of Lode parameter L for all values of χ. For example, in Fig. 5(b) where $\chi = 0.33$ the onset of tertiary creep, i.e. $\dot{E}_e/\dot{E}_{ss} > 5$, takes place at $t = 0.642 \times 10^7$s for $L = -1$ while it occurs at $t = 1.482 \times 10^7$s for $L = 1$. This sensitivity to the value of the Lode parameter decreases with increasing values of χ. For example, in Fig. 5(a) where $\chi = 3$, the onset of tertiary creep occurs at $t = 0.178 \times 10^7$s for $L = -1$ and at $t = 0.243 \times 10^7$s for $L = 1$. The analyses for $L = 0.5$ and $L = 1$ with $\chi = 0.33$ are terminated after void collapse.

Approved for public release; distribution unlimited.

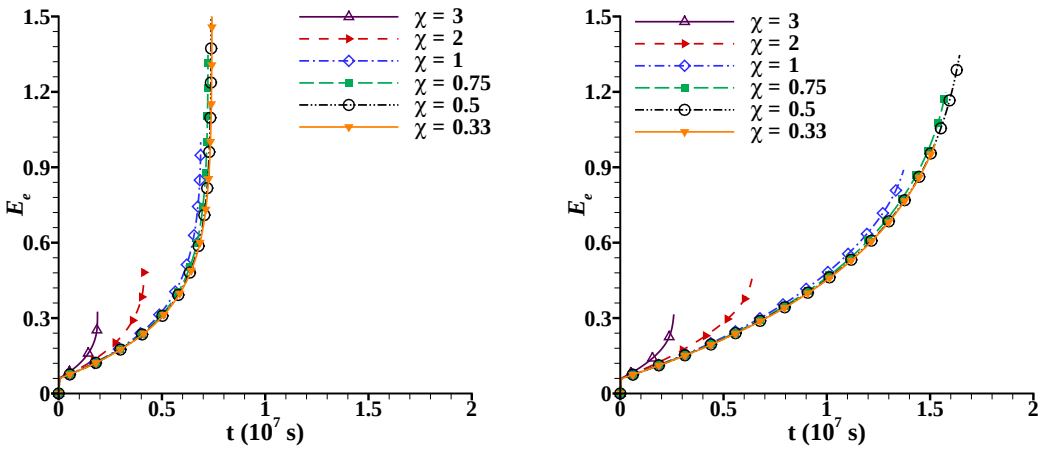

(a) Lode parameter $L = -1$ (b) Lode parameter $L = 1$

Figure 6. Time histories of macroscopic effective creep strain (E_e) under constant nominal stress creep loading for Lode parameter (a) $L = -1$ and (b) $L = 1$.

The time histories of the effective creep strain E_e for six values of χ and for Lode parameter values of $L = -1$ and $L = 1$ are shown in Fig. 6. For all values of the Lode parameter, a decreasing value of stress triaxiality decreases the creep rate and delays the onset of tertiary creep for $\chi \geq 1$. For $\chi \leq 1$ with $L = -1$, Fig. 6(a), the secondary creep rate, $\dot{E}_{ss} \approx 0.4 \times 10^{-7}\text{s}^{-1}$, and the onset of tertiary creep are nearly independent of χ. With $L = -1$ and $\chi \leq 1$ the onset of tertiary creep occurs at $t \approx 0.6 \times 10^7$s. For $L = -1$ the calculations for $\chi = 0.5$ and 0.33 were terminated at $E_e = 1.5$.

In Fig. 6(b) where $L = 1$ $\dot{E}_{ss} \approx 0.35 \times 10^{-7}\text{s}^{-1}$ for $\chi \leq 1$. The onset of tertiary creep takes place at $t = 1.34 \times 10^7$s for $\chi = 1$ and at $t = 1.48 \times 10^7$s for $\chi = 0.33$. With $L = 1$ void collapse occurs for $\chi = 0.5$ and 0.33.

One feature common to all cases analyzed, both constant true stress loading and constant nominal stress loading, and for values of the Lode parameter, is that for values of the stress triaxiality $\chi \geq 0.75$ the analyses were terminated due to necking down of the ligament between adjacent voids giving a 90% loss of ligament.

3.2. Evolution of the porosity

The void volume fraction is defined as $f = (V_{\text{cell}} - V_M)/V_{\text{cell}}$ where V_{cell} is the current cell volume and V_M is the current material volume (the small elastic volume change is neglected) and f/f_0 is the relative void volume fraction.

Plots of relative void volume fraction f/f_0 versus time are shown in Fig. 7 for $\chi = 3$. The evolution of porosity is essentially independent of the value of the Lode parameter L for constant true stress creep loading, Fig. 7(a), whereas there is a significant dependence on L for constant nominal stress creep loading, Fig. 7(b). The void growth rate initially decreases as creep deformation shifts from primary to secondary creep, reaches a minimum value and then increases. The onset of tertiary creep (as defined here) is marked by the circles in Fig. 7. The earliest onset of tertiary creep in Fig. 7(b) occurs for $L = -1$ and the latest for $L = 1$. Due to the increase in imposed true stress under constant nominal stress loading the void growth rate is greater at any given time than that under constant true stress loading.

With $\chi = 0.33$ in Fig. 8 the relative void volume fraction decreases after an initial increase. In Fig. 8

Approved for public release; distribution unlimited.

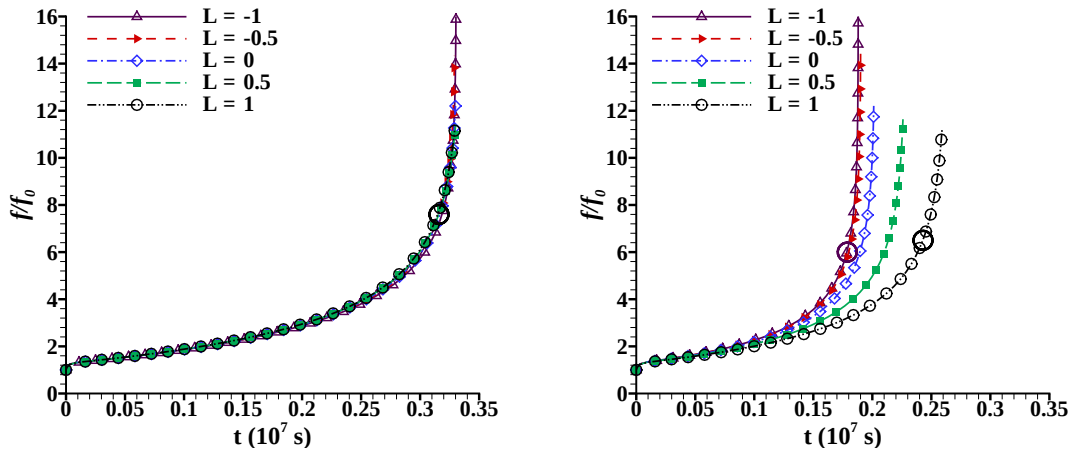

(a) Constant true stress creep loading for $\chi = 3$ (b) Constant nominal stress creep loading for $\chi = 3$

Figure 7. Plots of relative void volume fraction f/f_0 versus time t for stress triaxiality $\chi = 3$. (a) Constant true stress creep loading. (b) Constant nominal stress creep loading. The onset of tertiary creep for the Lode parameter values $L = -1$ and $L = 1$ is marked by a circle.

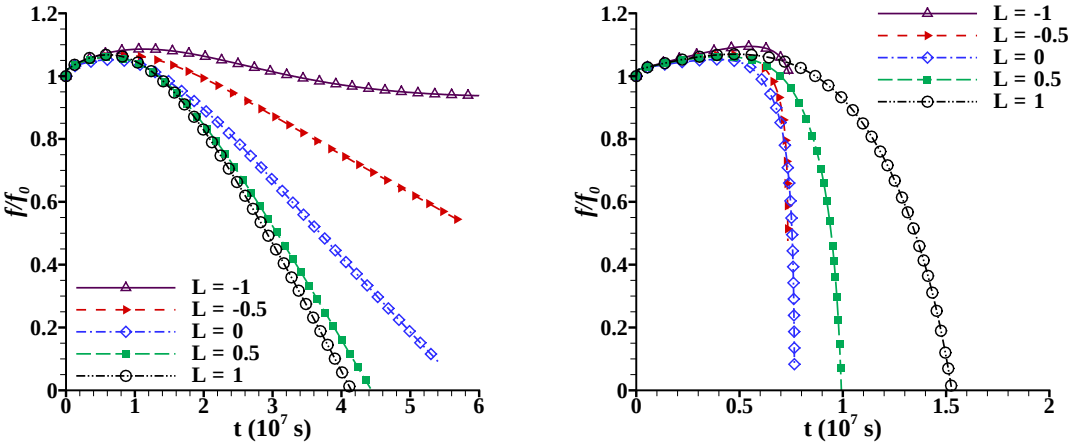

(a) Constant true stress creep loading for $\chi = 0.33$ (b) Constant nominal stress creep loading for $\chi = 0.33$

Figure 8. Plots of relative void volume fraction f/f_0 versus time t for stress triaxiality $\chi = 0.33$. (a) Constant true stress creep loading. (b) Constant nominal stress creep loading.

f/f_0 is independent of the value of the Lode parameter in the early stages of deformation. For $\chi = 0.33$ and $L = -1$ in Fig. 8(a), the relative void volume fraction increases to a maximum with $f/f_0 > 1$ and saturates to $f/f_0 \approx 1$. For $\chi = 0.33$ and $L \geq -0.5$, after an initial increase f/f_0 decreases. As seen in Fig. 8 f/f_0 decreases more rapidly under constant nominal stress loading than under constant true stress loading. This because under constant nominal stress loading the increasing value of Σ_1 leads to an increasing strain rate. The rate of decrease of porosity increases with increasing Lode parameter value

Approved for public release; distribution unlimited.

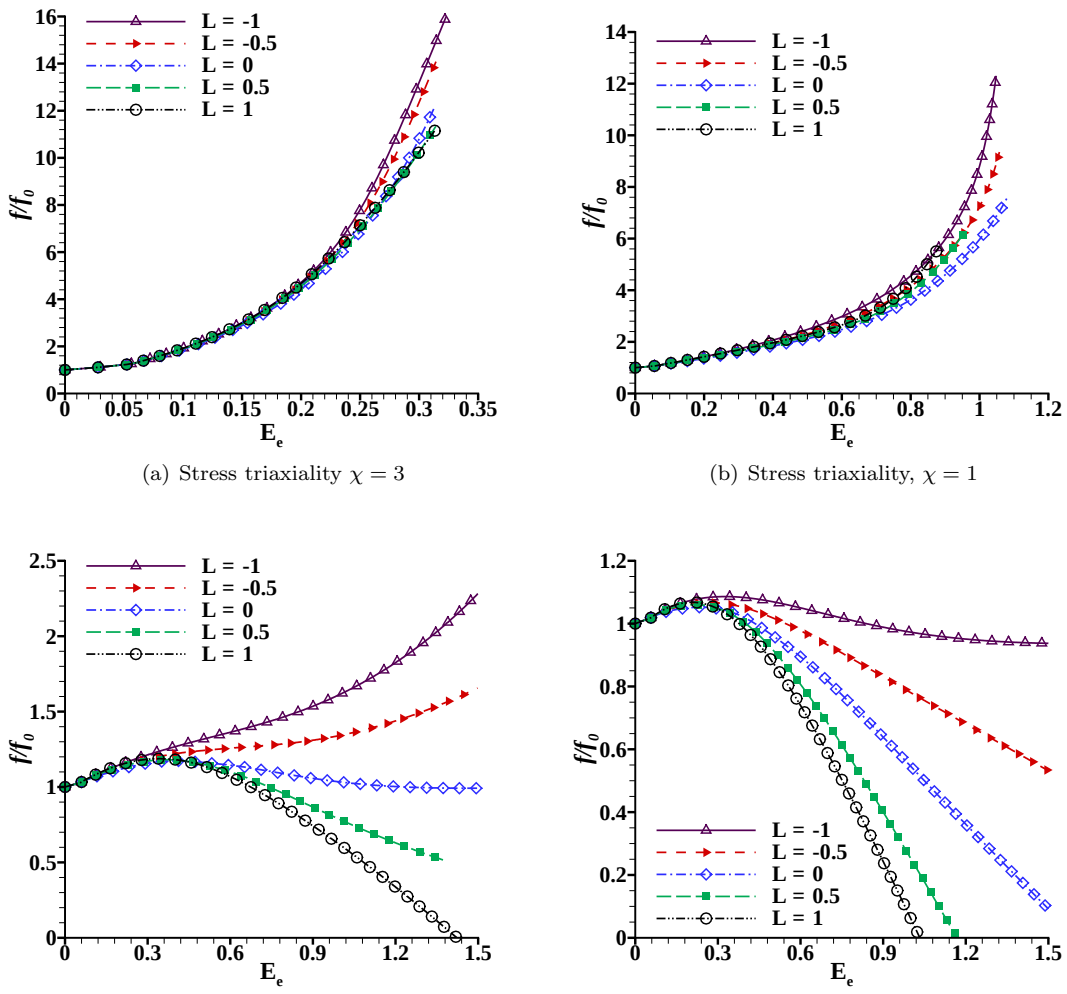

(a) Stress triaxiality $\chi = 3$

(b) Stress triaxiality, $\chi = 1$

(c) Stress triaxiality $\chi = 0.5$

(d) Stress triaxiality $\chi = 0.33$

Figure 9. Evolution of the relative void volume fraction f/f_0 as a function of the macroscopic effective creep strain E_e for various values of the stress triaxiality. (a) $\chi = 3$. (b) $\chi = 1$. (c) $\chi = 0.5$. (d) $\chi = 0.33$. The data is for constant true stress creep loading. However, the calculations for constant nominal stress loading give nearly the same results.

under constant true stress loading whereas the rate decreases with increasing value of Lode parameter under constant nominal stress loading. For instance the time to void collapse, $f/f_0 \approx 0$, under constant true stress loading for $L = -0.5$ is $t \approx 4.5 \times 10^7$s and for $L = 1$ it is $t \approx 4.2 \times 10^7$s. Under constant nominal stress loading the time to void collapse for $L = -0.5$ is $t \approx 1 \times 10^7$s and for $L = 1$ it is $t \approx 1.5 \times 10^7$s.

Figure 9 shows plots of relative void volume fraction f/f_0 versus macroscopic effective creep strain E_e under constant true stress loading. The corresponding results for constant nominal stress loading are nearly the same. For a given stress triaxiality the evolution of relative void volume fraction with respect to macroscopic creep deformation is not strongly dependent on the type of creep loading. Hence, the main difference between these two types of imposed loading is the different strain histories that occur.

Approved for public release; distribution unlimited.

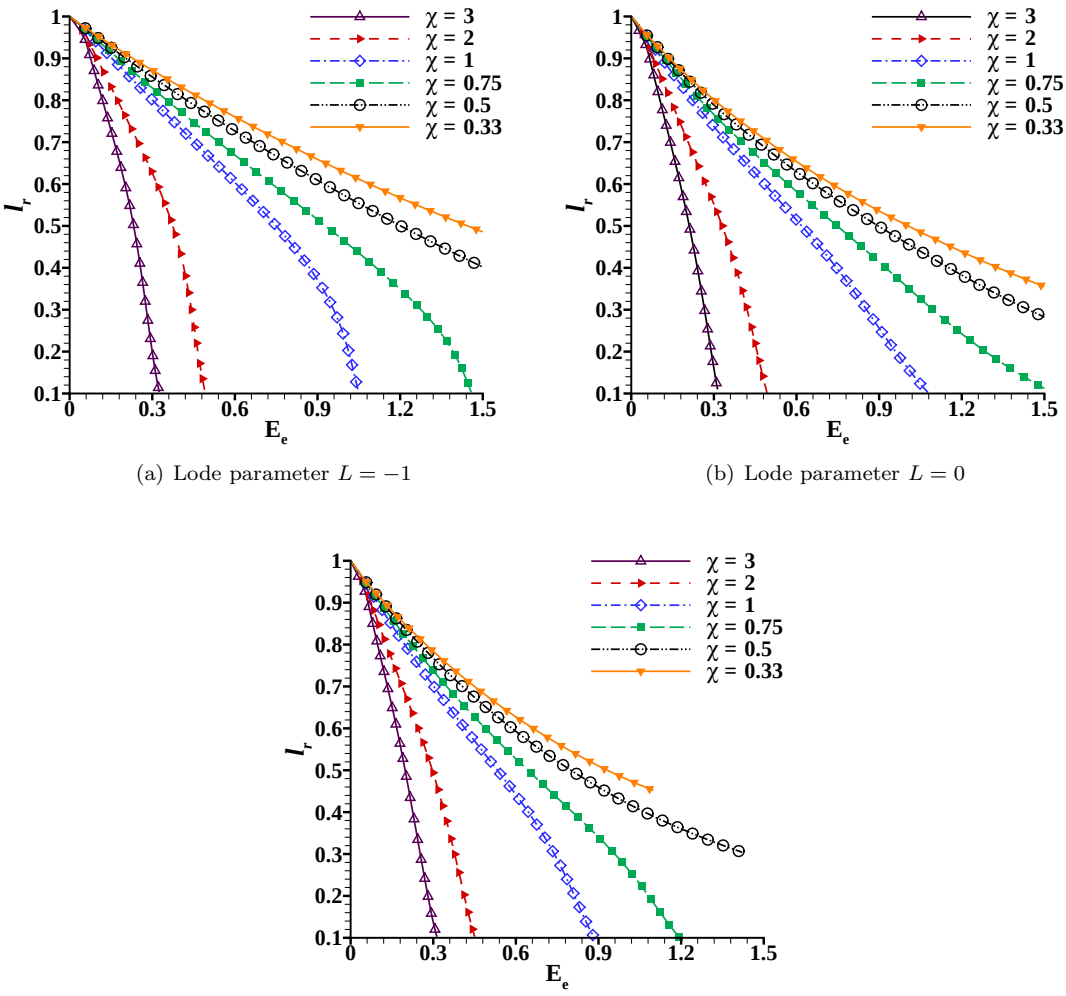

(a) Lode parameter $L = -1$

(b) Lode parameter $L = 0$

(c) Lode parameter $L = 1$

Figure 10. Progressive loss of relative ligament ($l_r = (a_3 - r_3)/(\tilde{a}_3 - \tilde{r}_3)$) in the x_3 direction under constant true stress creep loading for various values of the stress triaxiality χ and the Lode parameter L. (a) $L = -1$. (b) $L = 0$. (c) $L = 1$.

The evolution of the void volume fraction, at least with the constitutive description used in our analyses, mainly depends on the creep strain.

The evolution of porosity with E_e shows no dependence on the values of the Lode parameter until a stress triaxiality dependent value of E_e is reached. The value of E_e at which f/f_0 depends on the value of the Lode parameter increases with decreasing stress triaxiality until $\chi = 0.75$. For example, for $\chi = 3$ the effect of Lode parameter value is seen for $E_e > 0.25$ and for $\chi = 1$ the effect of Lode parameter value is seen for $E_e > 0.6$. On the other hand, the dependence of f/f_0 on the Lode parameter value for $\chi = 0.5$ occurs for $E_e > 0.3$ and for $\chi = 0.33$ this dependence can be seen for $E_e > 0.2$.

In Fig. 9(a) for $\chi = 3$, f/f_0 is maximum for $L = -1$ and minimum for $L = 1$ at any given $E_e > 0.25$. Whereas for $\chi = 1$ in Fig. 9(b) the value of f/f_0 is smaller for $L = 0$ than that for $L = \pm 1$ at any given

Approved for public release; distribution unlimited.

$E_e > 0.6$. For void growth in an fcc single crystal unit cell analyses under monotonically increasing load for $\chi \geq 1$ Wan et al. [29] and Yu et al. [35] observed a smaller void volume fraction at a given strain for $L = 0$ than for $L = \pm 1$. The analyses here for $\chi \geq 0.75$ were terminated after 90% loss of ligament and f/f_0 at the end of these analyses was found to decrease with increasing Lode parameter value. For example, for $\chi = 1$ and $L = -1$, 0 and 1, $f/f_0 = 12.3$, 7.6 and 5.71 at the end of the analysis, respectively.

In Fig. 9(c) where $\chi = 0.5$ void collapse occurs for $L = 1$ while in Fig. 9(d) where $\chi = 0.33$ void collapse occurs for both $L = 1$ and $L = 0.5$. In other cases in Figs. 9(c) and 9(d) the calculations were terminated on reaching $E_e = 1.5$. These results indicate that void collapse for $\chi = 0.5$ and 0.33, or an evolution toward void collapse can occur, for some values of Lode parameter at low values of stress triaxiality even when χ is positive. Budiansky et al. [36] found void collapse in an axisymmetric analysis of an isolated void in a power law creeping solid with $\Sigma_1 = \Sigma_2$ and $\Sigma_3/\Sigma_1 = -0.5$ which corresponds to $\chi = 0.33$ and $L = 1$.

The necking down between voids is quantified in terms of the evolution of the smallest ligament length between voids. For values of stress triaxiality and Lode parameter analyzed here the x_3 direction is the direction with the minimum value of Σ_i, Table. 1, and necking down between voids generally takes place in the x_3 direction. With $L = -1$ $\Sigma_2 = \Sigma_3$ and there is simultaneous necking down in the x_2 and x_3 directions. However, the ligament length in the x_3 direction can still be used to characterize necking.

The relative ligament length in this direction is $l_r = (a_3 - r_3)/(\tilde{a}_3 - \tilde{r}_3)$, where a_3 and r_3 are, respectively, the current cell length and void size along the x_3-axis, and $\tilde{a}_3$ and $\tilde{r}_3$ are, respectively, the cell length and void size along the x_3-axis after the first elastic step. Plots of l_r versus E_e are shown in Fig. 10 for $L = -1$, 0 and 1. The results in Fig. 10 are shown for constant true stress creep loading. The results for constant nominal stress creep loading are nearly the same.

There is a significant difference between the responses with $L = -1$ and $L = 1$ in Fig. 10. With $L = -1$, $\Sigma_2 = \Sigma_3$ there is simultaneous necking in the ligament between adjacent voids in the x_2 and x_3 directions, whereas for $L = 1$, $\Sigma_1 = \Sigma_2$ necking between adjacent voids only occurs in the x_3 direction. The necking down of the ligament is mainly responsible for the rapid increase in void growth rate during tertiary creep regime for $\chi = 3$ and 2 and, as discussed, void growth occurs more slowly with strain with increasing Lode parameter value.

Figure 10 shows the variation of the ligament length l_r for $L = -1$, 0 and 1. For $\chi \geq 0.75$ l_r decreases to ≈ 0.1 for $E_e \leq 1.5$. There is, as expected, a strong dependence on the strain to reach $l_r = 0.01$ on the value of χ. For $L = -1$ a strain is reached at which l_r decreases rapidly for $\chi \geq 0.75$. For $L = 1$ this rapid decrease only occurs for $\chi = 3$ and 2 although there is an increases in the magnitude of the slope for $\chi = 1$ and (slightly) for $\chi = 0.75$. For $L = 0$, there is only a rapid increase in slope magnitude for $\chi = 3$ and 2; for $\chi = 1$ and 0.75 there is a very gradual decrease in ligament which is associated with the Poisson area reduction with increasing strain rather than a more or less abrupt necking down. The results show that under creep loading there is a gradual transition depending on stress triaxiality and Lode parameter between necking down between voids that can occur at relatively small strains and a gradual decrease in distance between voids that requires much larger strains.

3.3. Evolution of the void shape

We characterize the void shape by two ratios: (i) r_3/r_1 where r_1 is the void size along the x_1-axis and r_3 is the void size along the x_3-axis; and (ii) r_3/r_2 where r_2 is the void size along the x_2-axis. The ratio r_3/r_1 gives the gives the ratio of the minimum cross sectional radius to that in the loading direction while r_3/r_2 is the ratio of the void sizes along the coordinate axes in the plane perpendicular to the loading direction.

Figure 11 shows the evolution of the radius ratios with effective creep strain E_e for $L = -1$ and for constant true stress loading (the curves for both constant true stress and constant nominal stress loading are essentially identical). In Fig. 11(a) for $\chi \geq 2$ the ratio r_3/r_1 initially decreases and then increases indicating the necking down of the ligament between adjacent voids. For $\chi = 1$ there is an increase in

Approved for public release; distribution unlimited.

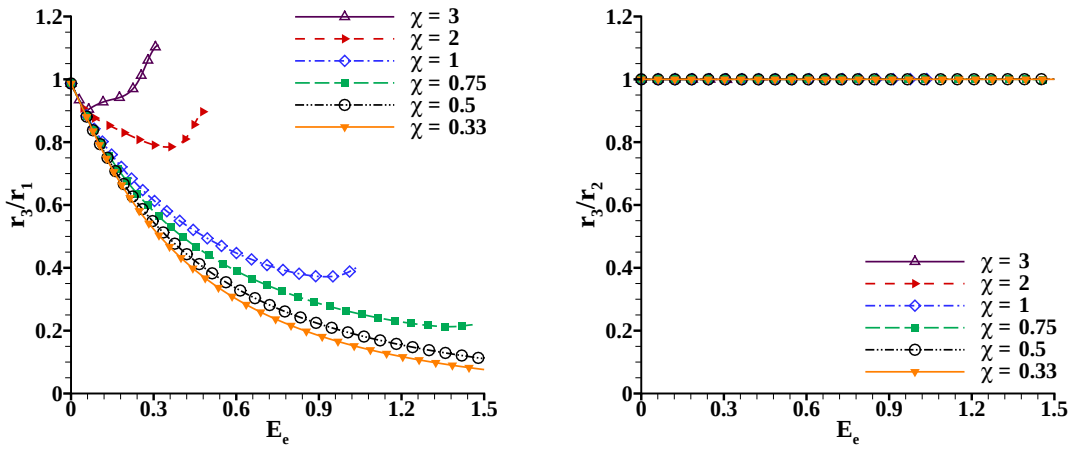

(a) r_3/r_1 (b) r_3/r_2

Figure 11. Evolution of void radius ratios for various values of the stress triaxiality χ with the Lode parameter $L = -1$. (a) r_3/r_1. (b) r_3/r_2.

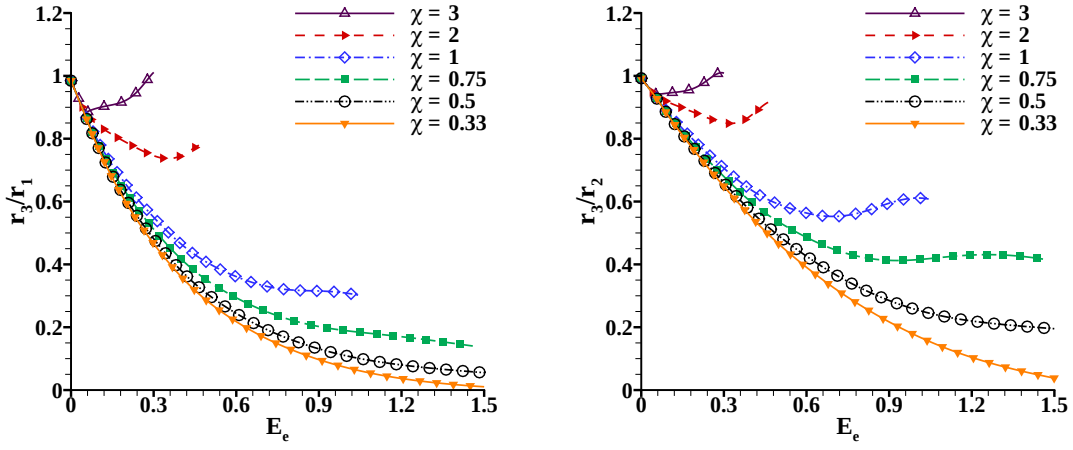

(a) r_3/r_1 (b) r_3/r_2

Figure 12. Evolution of void radius ratios for various values of the stress triaxiality χ with the Lode parameter $L = 0$. (a) r_3/r_1. (b) r_3/r_2.

r_3/r_1 just before the calculation is terminated at $E_e \approx 1$. For smaller values of χ the value of r_3/r_1 monotonically decreases during the deformation history so that the void becomes prolate.

The value of the Lode parameter $L = -1$ corresponds to an axisymmetric state of stress, $\Sigma_1 > \Sigma_2 = \Sigma_3$, with the x_1-axis being the symmetry axis. The radius ratio r_3/r_2 remains close to unity, Fig. 11(b), for the range of stress triaxiality values analyzed in the current work. However the void cross sectional shape depends on the stress triaxiality value. For $\chi = 0.33$, where void interaction effects are not significant and no necking down of the ligament between voids occurs, the cross sectional shape

Approved for public release; distribution unlimited.

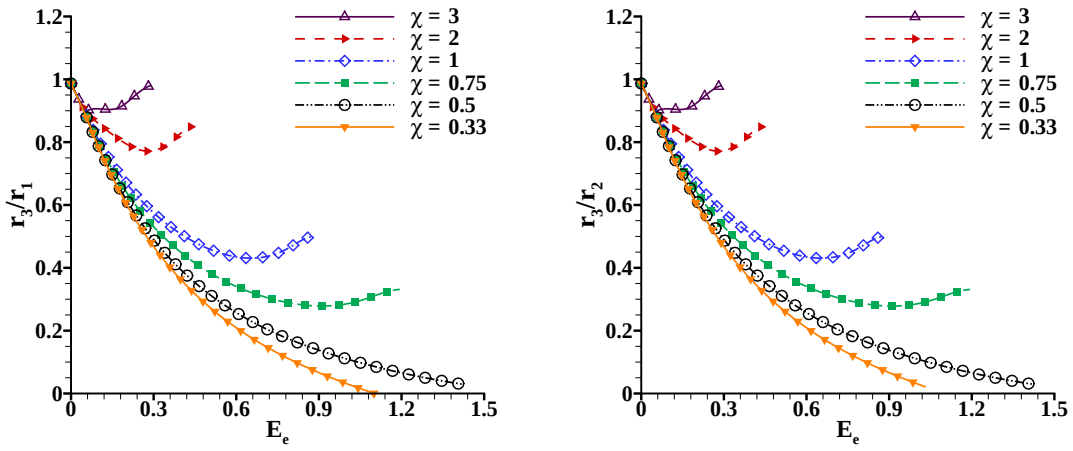

(a) r_3/r_1 (b) r_3/r_2

Figure 13. Evolution of void radius ratios for various values of the stress triaxiality χ with the Lode parameter $L = 1$. (a) r_3/r_1. (b) r_3/r_2.

remains essentially circular. For $\chi = 3$ necking down of the ligament in the x_2 and x_3 directions leads to a rapid increase in the void radii in these directions whereas void growth in off-axis directions is less so that the void cross section is not circular. The largest deviation from a circle occurs at 45°. For example, the radius ratio $r_{45^\circ}/r_3 = 0.91$ for $\chi = 3$ and $L = -1$ at an effective creep strain $E_e = 0.322$ which is when there is 90% loss of ligament.

For $L = 0$, Fig. 12, r_3/r_1 and r_3/r_2 decrease initially for $\chi \geq 2$ but then increase for $L = -1$. For $\chi = 1$ both radius ratios eventually level off while for $\chi = 0.5$ and 0.33 the void predominantly elongates in the x_1 direction which is the major stress axis. Both r_3/r_1 and r_3/r_2 approach zero with $\chi = 0.33$ indicating void collapse.

The trends for the variation of r_3/r_1 and r_3/r_2 for $L = 1$ in Fig. 13 are qualitatively similar to those for $L = 0$ in Fig. 12 but with void collapse occurring for $\chi = 0.5$ as well as for $\chi = 0.33$. For $\chi = 1$ and 0.75, the radius ratio r_3/r_1 increases due to void interaction effects in the x_3 direction, but the values remain well below unity over the entire deformation history leading to the formation of an oblate shape (largest cross section perpendicular to the direction of loading). Although not shown here $r_2/r_1 \approx 1$ throughout the deformation history for all values of stress triaxiality χ for $L = 1$ since the x_3-axis is the axis of symmetry, with $\Sigma_1 = \Sigma_2$. It is worth noting that for high stress triaxiality, $\chi \geq 2$, the void radii along all three axes increase for all Lode parameter values. For smaller values of χ, r_3 decreases during the deformation history so that the void becomes oblate.

Figure 14 shows the void shapes obtained for $L = -1$, 0 and 1 and for three values of stress triaxiality $\chi = 3$, 1 and 0.33. For all values of L, the void is essentially spherical for $\chi = 3$. For $L = -1$ and $\chi = 1$ the void is a prolate spheroid (largest cross section along the loading direction) and needle-like for $\chi = 0.33$. For $L = 0$ the void has a three dimensional shape for $\chi = 1$ and is like an elliptical crack for $\chi = 0.33$. For $L = 1$ the void evolves into a shape like that of an oblate spheroid for $\chi = 1$ and like that of a penny shaped crack for $\chi = 0.33$ (and also for $\chi = 0.5$ not shown here).

17
Approved for public release; distribution unlimited.

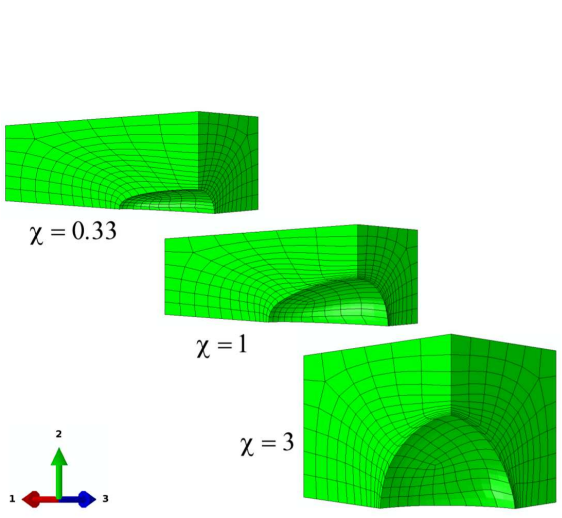

(a) Lode parameter, $L = -1$

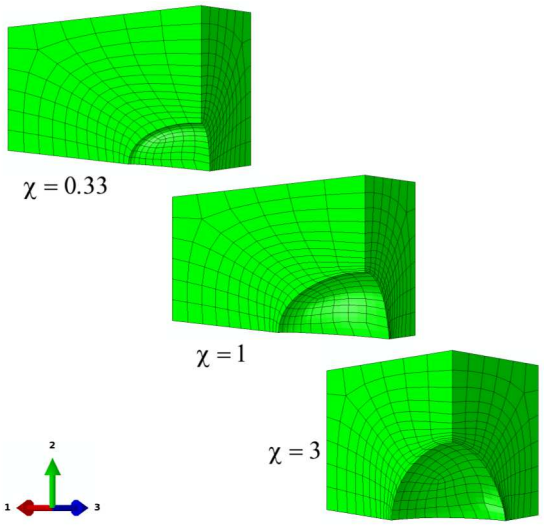

(b) Lode parameter, $L = 0$

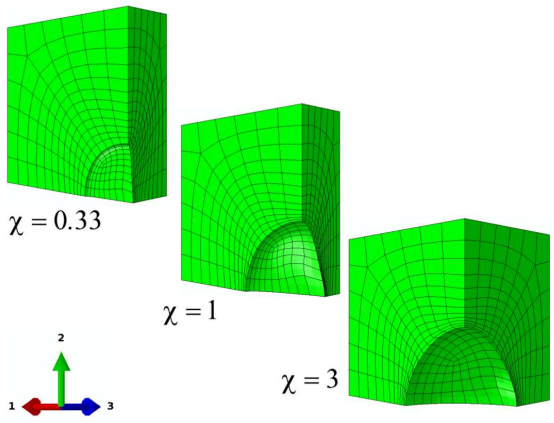

(c) Lode parameter, $L = 1$

Figure 14. The void shape for various values of the Lode parameter for $\chi = 0.33$ at $E_e = 0.8$, $\chi = 1$ at $E_e = 0.8$ and $\chi = 3$ at $E_e = 0.3$. (a) $L = -1$. (b)$L = 0$. (c)$L = 1$.

3.4. Stress distributions

Distributions of σ_{11} normalized by the current value of the applied stress Σ_1 for $\chi = 0.33$ are shown in Fig. 15. Figure 15(a) shows distributions for $L = -1$ and Fig. 15(b) for $L = 1$. The value of Σ_1 is constant throughout the deformation history under constant true stress loading but the value of Σ_1 changes with the change in cross sectional area under constant nominal stress loading. For both types of imposed loading the distributions of σ_{11}/Σ_1 at a given value of E_e are nearly same and the distributions in Fig. 15 (and in Fig. 16) are for constant Σ_1 loading. The three values of strain shown in Fig. 15 are: (i) after the first elastic step, denoted as $E_e = 0$; (ii) at $E_e = 0.2$; and (iii) at $E_e = 0.8$.

After the first elastic step, $\Sigma_1 = 750$MPa and the maximum value of the stress ratio, σ_{11}/Σ_1 is 1.77. This maximum occurs at the circumference of the void on the $x_2 - x_3$ plane. For $L = -1$ at $E_e = 0.2$ in Fig. 15(a) the maximum value of σ_{11}/Σ_1 has decreased to 1.29. This corresponds to maximum

Approved for public release; distribution unlimited.

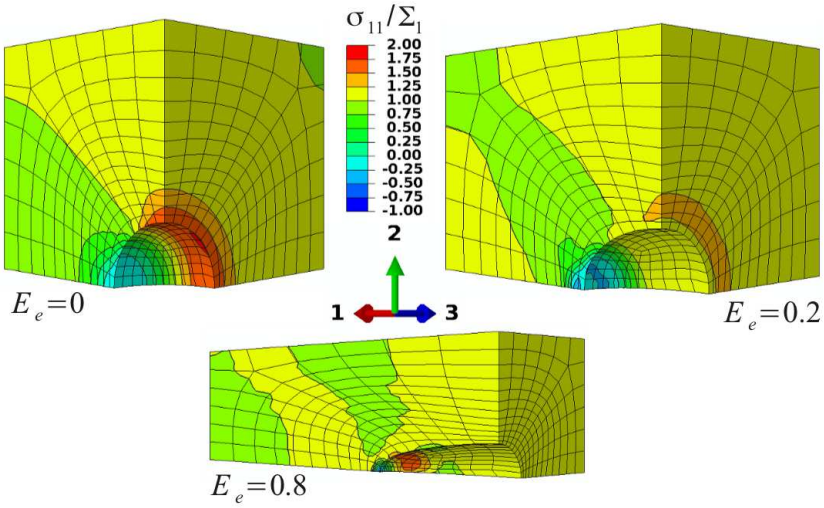

(a) Lode parameter, $L = -1$

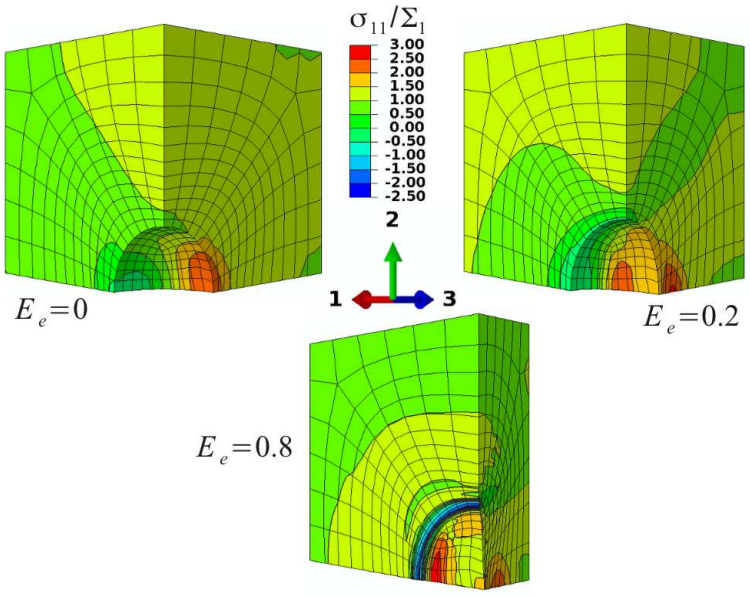

(b) Lode parameter, $L = 1$

Figure 15. Distributions of normalized stress σ_{11}/Σ_1 after the first elastic step and at $E_e = 0.2$ and 0.8 under constant true stress creep loading for stress triaxiality $\chi = 0.33$. (a) $L = -1$. (b) $L = 1$.

$\sigma_{11} = 968$MPa under constant true stress loading but to 1189MPa under constant nominal stress loading since Σ_1 has increased to 922MPa due to the reduction in cross sectional area. At $E_e = 0.8$ the maximum stress concentration has shifted towards the tip of the void which has taken on a needle-like shape and the maximum value of σ_{11}/Σ_1 is 1.63. The maximum σ_{11} under constant true stress creep loading is 1222MPa and is 2.69GPa under constant nominal stress loading since $\Sigma_1 = 1.65$GPa at $E_e = 0.8$.

For $\chi = 0.33$ and $L = 1$, Fig. 15(b), $\Sigma_1 = 500$MPa after the first elastic step and the peak value of σ_{11}/Σ_1 is 2.37 and occurs at the circumference of the void in $x_2 - x_3$ plane. Under constant nominal stress

Approved for public release; distribution unlimited.

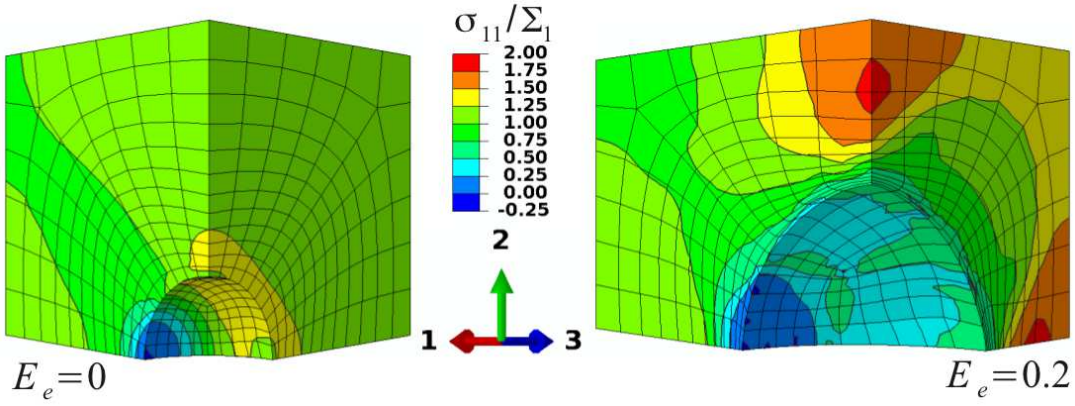

(a) Lode parameter, $L = -1$

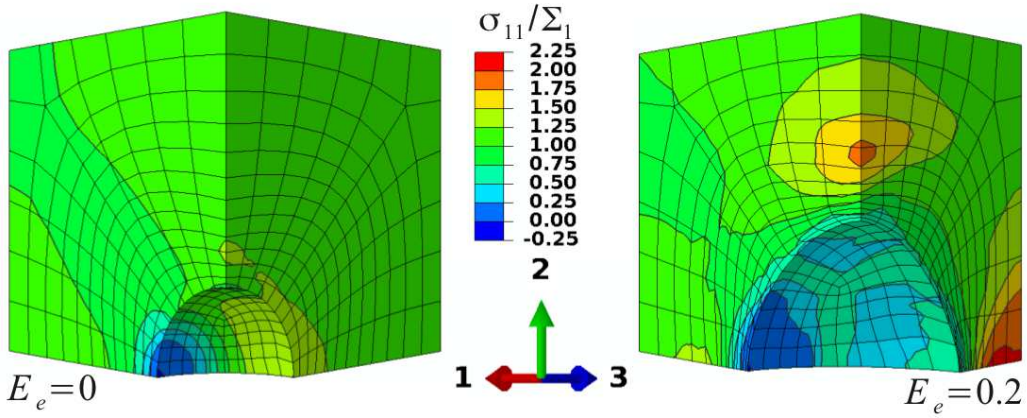

(b) Lode parameter, $L = 1$

Figure 16. Distributions of normalized stress σ_{11}/Σ_1 after the first elastic step and at $E_e = 0.2$ under constant true stress creep loading for stress triaxiality $\chi = 3$. (a) $L = -1$. (b) $L = 1$.

creep, Σ_1 increases to 554MPa at $E_e = 0.2$. At $E_e = 0.2$ the maximum stress concentration is still on the $x_2 - x_3$ plane but has slightly shifted away from the void surface and has increased to $\sigma_{11}/\Sigma_1 = 2.66$ so that the maximum values of σ_{11} are 1.33GPa and 1.47GPa for constant true stress and constant nominal stress loading, respectively. For $\chi = 0.33$ and $L = 1$ at $E_e = 0.8$, void collapse has led to the void evolving into a shape like that of a penny shaped crack. The maximum value of σ_{11}/Σ_1 has increased to 2.79 and occurs near the tip. Under constant nominal stress loading $\Sigma_1 = 751$MPa at $E_e = 0.8$ leading to $\sigma_{11} = 2.10$GPa at the point of maximum stress concentration while $\sigma_{11} = 1.40$GPa for constant true stress loading.

Distributions of σ_{11}/Σ_1 for $\chi = 3$ and $L = -1$ and $L = 1$ are shown in Fig. 16. At $E_e = 0$ $\Sigma_1 = 2750$MPa for $L = -1$ and $\Sigma_1 = 2500$MPa for $L = 1$; the maximum value, $\sigma_{11}/\Sigma_1 = 1.48$, is the same for both $L = -1$, Fig. 16(a), and $L = 1$, Fig. 16(b). At $E_e = 0.2$ the peak value of σ_{11}/Σ_1 is 1.83 for $L = -1$ and 2.11 for $L = 1$. For $L = -1$ the maximum value occurs at the center of the ligament between adjacent voids along both the x_2 and x_3 axes, Fig. 16(a). For $L = 1$ at $E_e = 0.2$ the maximum value is attained only along the x_3 axis. At $E_e = 0.2$ the maximum stress values are 5.0GPa for $L = -1$ and 5.3GPa for $L = 1$ under constant true stress loading.

Approved for public release; distribution unlimited.

4. Discussion

Our analyses were motivated by the experiments in [1,2] on creep of a nickel based single crystal superalloy under uniaxial tensile loading. Since our aim is to model porosity evolution in creep we considered applied stresses (of one kind or another) not varying with time. In the experiments the applied nominal stress was fixed so that type of loading was imposed in our calculations. However, for comparison purpose as well as to provide a basis for developing a phenomenological creep damage constitutive relation the response under time constant true stresses applied to the unit cell was also analyzed. This latter type of loading is analogous to the type of loading applied in the ductile fracture oriented studies. Although the imposed loading in the crystals tested in [1,2] was uniaxial tension, say due to constraint or inhomogeneity effects, the stress state can differ and, in particular, there can be regions of locally enhanced stress triaxiality as well as local variations in the value of the Lode parameter.

The calculations show that the time history of deformation and porosity depends on which type of creep loading is imposed. However, when the evolution of void volume fraction and shape is considered as a function of a measure of the overall creep strain, the results from the two types of imposed loading essentially coincide. This is not particularly surprising because (except for the effect of elasticity) the slip system resolved shear stress-resolved shear strain relation is history independent. If the slip system flow rule were strongly history dependent this conclusion would not hold. Another simplification in the crystal constitutive relation is that only self hardening has been considered. It is worth noting that with porosity evolution considered as a function of strain, our results exhibit many of the same qualitative features regarding the dependence on stress triaxiality and Lode parameter values as those found in ductile fracture oriented cell model studies.

In our analyses we have considered one value of initial applied Mises effective stress. The initial applied Mises effective stress is time independent under constant true stress creep loading whereas it increases with time under constant nominal stress creep loading. In the absence of experimental creep data at different stress levels at 760°C for the material tested in [1,2] we used a representative value for the secondary creep slip system power law exponent. Since, at least with this constitutive characterization, the creep response is essentially history independent and the void shape changes mainly occur when the material is in the secondary creep regime, we expect that the macroscopic stress dependence will exhibit this same power law relation. Additional parameter studies are needed to determine the orientation dependence of the porosity evolution. The results of such analyses together with the constant true stress results obtained here could provide the background for developing a phenomenological constitutive relation using a framework such as in [47].

We have used the Lode parameter to characterize the role of the third invariant of the applied stress. Another parameter that could be used for that purpose is the parameter ω in Nahshon and Hutchinson [20] which has the convenient feature that it lies between zero and one. The value of ω is zero for all axisymmetric stress states. The value of the Lode parameter can be 1 or -1 for an axisymmetric stress state (two of the applied stresses on the unit cell equal). Our three dimensional analysis of void growth showed that significantly different void evolution histories are possible for $L = 1$ and $L = -1$ because the results depend on which plane contains the two equal stresses.

Budiansky et al. [36] found that an isolated initially spherical void in an isotropic matrix under power law creep for high stress triaxiality tends to become a prolate spheroid for stress ratios giving $L = -1$ whereas it tends to become an oblate spheroid for stress ratios giving $L = 1$. Here, for those loading conditions the same shape evolution occurs until void interaction effects come into play and the void aspect ratio then tends to increase and three dimensional void growth is observed. Similar void interaction effects were seen in [39] for an initially spherical void in an isotropic axisymmetric ($L = -1$) unit cell under power law creep at high stress triaxiality. For uniaxial tension with $\chi = 0.33$ and $L = -1$, Budiansky et al. [36] found that the void predominantly elongates in the loading direction leading to a needle-like shape. Whereas for $\chi = 0.33$ and $L = 1$ the void collapses forming a penny-shaped crack. In our cell model calculations at low stress triaxiality values void interaction effects are not dominant and

Approved for public release; distribution unlimited.

the void shape in our analyses evolves as in [36].

With reducing thickness of the sheet specimens Srivastava et al. [1] found that local cleavage played a significant role in the observed creep rupture process whether environmental effects were dominant or not. Our analyses suggest that the high local stresses that develop in the ligament between voids could precipitate cleavage which would lead to an abrupt loss of load carrying area. This then would increase the stress on the remaining load carrying material and so act to precipitate further cleavage. This loss of area would be more damaging for thinner cross-sections. This could account for a thickness debit effect in Ni-based single crystal superalloys in circumstances where surface damage effects do not come into play.

5. Conclusions

Finite deformation finite element analyses of void growth in an fcc crystal under isothermal creep loading conditions were carried out. The slip system constitutive relation modeled primary and secondary creep. A unit cell was analyzed for crystals with a $< 001 >$ orientation and with a fixed initial void volume fraction of 0.01. The effect of stress triaxiality values (the ratio of mean normal true stress to Mises effective stress) between 0.33 and 3 and Lode parameter values between -1 and 1 was considered for both constant applied true stress loading and for constant applied nominal stress loading. For both types of loading proportional true stress ratios were maintained. The results show that:

1. For fixed values of the stress triaxiality and Lode parameter, the mode of creep loading (constant applied true stress or constant applied nominal stress) has a significant effect on the time histories of the macroscopic effective creep strain and the void volume fraction. This dependence is more pronounced at low values of the stress triaxiality.
2. The effect of imposed loading type stems from the loading mode dependence of the macroscopic effective creep strain. The dependence of the void volume fraction and shape evolution on the macroscopic effective creep strain is independent of whether constant true stress or constant nominal stress creep loading is applied. The main features of this dependence are similar to the observations in previous cell model analyses of void growth under monotonically increasing loading.
3. There is no significant effect of the value of the Lode parameter at high values of the stress triaxiality. At low values of the stress triaxiality the evolution of void volume fraction (including whether or not void collapse occurs) and the void shape evolution can be strongly dependent on the Lode parameter value.
4. Due to void growth and the change in void shape the local stress magnitude in the void vicinity generally increases with time. For low values of the stress triaxiality, stress concentration factors exceeding 2.5 were found.
5. A possibility, for certain materials, is that locally high stresses could initiate cleavage before void coalescence occurs. The associated loss of stress carrying capacity would be more pronounced for thinner specimens and this could lead to a thickness debit effect.

Acknowledgments

We are grateful for the financial support provided by the Air Force Research Laboratory (AFRL/RXLM) to the University of North Texas under the Institute for Science and Engineering Simulation (ISES) Contract FA8650-08-C-5226.

6. References

[1] Srivastava A., Gopagoni S., Needleman A., Seetharaman V., Staroselsky A. and Banerjee R., 2011. Effect of specimen thickness on the creep response of a Ni-base single crystal superalloy. in preparation.

22
Approved for public release; distribution unlimited.

[2] Seetharaman V. and Cetel A.D., 2004. Thickness debit in creep properties of PWA1484. Superalloys 2004, Edited by K.A. Green, T.M. Pollock and H. Harada, TMS (The Minerals, Metals & Materials Society), 207-214.
[3] Anton D.L. and Giamei A.F., 1985. Porosity distribution and growth during homogenization in single crystals of a nickel-base superalloy. Materials Science and Engineering, 76, 173-180.
[4] Link T., Zabler S., Epishin A., Bansal M. and Thibault X., 2006. Synchrotron tomography of porosity in single crystal nickel-base superalloys. Materials Science and Engineering: A, 425, 47-54.
[5] Baldan A., 1995. On the thin-section size dependent creep strength of a single crystal nickel-base superalloy. Journal of materials science, 30, 6288-6298.
[6] Hüttner R., Gabel J., Glatzel U. and Völkl R., 2009. First creep results on thin-walled single-crystal superalloys. Material science and engineering A, 510-511, 307-311.
[7] Gullickson J., Needleman A., Staroselsky A. and Cassenti B., 2008. Boundary damage effects on the evolution of creep strain. Modelling and Simulation in Material Science and Engineering, 16, 075009.
[8] Cassenti B. and Staroselsky A., 2009. The effect of thickness on the creep response of thin-wall single crystal components. Materials Science and Engineering: A, 508(1-2), 183-189.
[9] Bensch M., Preußner J., Hüttner R., Obigodi G., Virtanen S., Gabel J. and Glatzel U., 2010. Modelling and analysis of the oxidation influence on creep behaviour of thin-walled strutures of the single-crystal nickel-base superalloy René N5 at 980°C. Acta Materialia, 58, 1607-1617.
[10] Needleman A., 1972. Void growth in an elasticplastic medium. Journal of Applied Mechanics, 39, 964970.
[11] Tvergaard V., 1981. Influence of voids on shear band instabilities under plane strain conditions. Internation Journal of Fracture, 17, 389-407.
[12] Tvergaard V., 1982. On localization in ductile materials containing spherical voids. Internation Journal of Fracture, 18, 237-252.
[13] Koplik J. and Needleman A., 1988. Void growth and coalescence in porous plastic solids. International Journal of Solids and Structures, 24, 835853.
[14] Worswick M.J. and Pick P.J., 1990. Void growth and constitutive softening in a periodically voided solid. Journal of Mechanics and Physics of Solids, 38, 601-625.
[15] Faleskog J. and Shih C.F., 1997. Micromechanics of coalescence-I. Synergistic effects of elasticity, plastic yielding, and multi-size-scale voids. Journal of Mechanics and Physics of Solids, 45, 21-50.
[16] Pardoen T. and Hutchinson J.W., 2000. An extended model for void growth and coalescence. Journal of Mechanics and Physics of Solids, 48, 2467-2512.
[17] Horstemeyer M.F. and Ramaswamy S., 2000. On factors affecting localization and void growth in ductile metals: a parametric study. International Journal of Damage Mechanics, 9, 528.
[18] Zhang K.S., Bai J.B. and Francois D., 2001. Numerical analysis of the influence of the Lode parameter on void growth. International Journal of Solids and Structure,s 38, 58475856.
[19] Gao X. and Kim J., 2006. Modeling of ductile fracture: significance of void coalescence. International Journal of Solids and Structures, 43, 62776293.
[20] Nahshon K. and Hutchinson J.W., 2008. Modification of the Gurson model for shear failure. European Journal of Mechanics A/Solids, 27, 1-17.
[21] Barsoum I. and Faleskog J., 2011. Micromechanical analysis on the influence of the Lode parameter on void growth and coalescence. International Journal of Solids and Structures, 48, 925-938.
[22] Bao Y. and Wierzbicki, T., 2004. On fracture locus in the equivalent strain and stress triaxiality space. International Journal of Mechanical Sciences, 46, 81-98.
[23] Hori M. and Nemat-Nasser S., 1988. Mechanics of void growth and void collapse in crystals. Mechanics of Materials, 7, 1-13.
[24] O'Regan T.L., Quinn D.F., Howe M.A. and McHugh P.E., 1997. Void growth simulations in single crystals. Computational Mechanics, 20, 115121.
[25] Orsini V.C. and Zikry M.A., 2001. Void growth and interaction in crystalline materials. International Journal of Plasticity, 17, 1393-1417.
[26] Potirniche G.P., Hearndon J.L., Horstemeyer M.F. and Ling X.W., 2006. Lattice orientation effects on void growth and coalescence in fcc single crystals. International Journal of Plasticity, 22, 921-942.
[27] Kysar J.W., Gan Y.X. and Mendez-Arzuza G., 2005. Cylindrical void in a rigid-ideally plastic single crystal. Part I: Anisotropic slip line theory solution for face-centered cubic crystals. International Journal of Plasticity, 21(8), 1481-1520.
[28] Schacht T., Untermann N. and Steck E., 2003. The influence of crystallographic orientation on the deformation behavior of single crystals containing microvoids. International Journal of Plasticity, 19, 1605-1626.
[29] Wan J.S., Yue Z.F. and Lu Z.Z., 2005. Casting microporosity growth in single-crystal superalloys by a three dimensional unit cell analysis. Modelling and Simulation in Material Science and Engineering, 13, 875-892.
[30] Wan J.S., Lu Z.Z. and Yue Z.F., 2006. Growth of casting microcrack and micropore in single crystal superalloys analysed by three dimensional unit cell. Journal of Material Science and Technology, 2, 183-189.
[31] Liu W.H., Zhang X.M., Tang J.G. and Du Y.X., 2007. Simulation of void growth and coalescence behavior with 3D crystal plasticity theory. Computational Materials Science, 40, 130-139.
[32] Yang M. and Dong X., 2009. Simulation of lattice orientation effects on void growth and coalescence by crystal plasticity.

Approved for public release; distribution unlimited.

Acta Metallurgica Sinica (English Letters), 22(1), 40-50.
[33] Sangyul H. and Kim K., 2010. Void growth and coalescence in fcc single crystals. International Journal of Mechanical Sciences, 52, 863-873.
[34] Yerra S.K., Tekoglu C., Scheyvaerts F., Delanny L., Van Houtte P. and Pardoen T., 2010. Void growth and coalescence in single crystals. International Journal of Solids and Structures, 47, 1016-1029.
[35] Yu Q.M., Hou N.X. and Yue Z.F., 2010. Finite element analysis of void growth behavior in nickle-based single crystal superalloys. Comutational Materials Science, 48, 597-608.
[36] Budiansky B., Hutchinson J.W. and Slutsky S., 1982. Void growth and collapse in viscous solids, Mechanics of solids (ed. H.G. Hopkins and M.J. Sewell), Oxford: Pregamon Press, 13-45.
[37] Dennis, R. J., Mechanistic modelling of deformation and void growth behaviour in superalloy single crystals, PhD thesis, Imperial College London, 2000.
[38] Busso E.P., O'Dowd N.P. and Dennis R.J., 2001. A rate dependent formulation for void growth in single crystal materials. IUTAM Sympossium on Creep in Structurees (eds. S. Murakani and N.Ohno), Kluwer Academic Publishers, 41-50.
[39] Needleman A., Tvergaard V., and Van der Giessen E., 1995. Evolution of void shape and size in creeping solids. International Journal of Damage Mechanics, 4, 134-152.
[40] Needleman A. and Rice J.R., 1980. Plastic creep flow effects in the diffusive cavitation of grain boundaries. Acta Metallurgica, 28(10), 1315-1332.
[41] Cocks A.C.F. and Ashby M.F., 1982. On creep fracture by void growth, Progress in Materials Science, 27, 189-244.
[42] Huang Y., 1991. Harvard University Report Mech-178.
[43] Kysar J.W., 1997. unpublished report.
[44] Asaro R.J. and Needleman A., 1985. Texture development and strain hardening in rate dependent polycrystals. Acta Metallurgica, 33, 923-953.
[45] Asaro R.J., 1983. Crystal plasticity. Journal of Applied Mechanics, 50, 921-934.
[46] ABAQUS User's Manual, version 6.6 (2006), ABAQUS Inc., Providence, RI.
[47] Danas K. and Ponte Castaneda P., 2009. A finite strain model for anisotropic viscoplastic porous media: I - Theory. European Journal of Mechanics, A/Solids, 28, 387-401.

Approved for public release; distribution unlimited.